Applied Geochemistry 2020

https://doi.org/10.1016/j.apgeochem.2020.104538

Micro-X-ray diffraction and chemical mapping of aged interfaces between cement pastes and Opalinus Clay

Ellina Bernard[a)], Andreas Jenni[a)], Martin Fisch[a)], Daniel Grolimund[b)], Urs Mäder[a)].

[a)] University of Bern, Institute of Geological Sciences, Rock-Water Interaction, 3012 Bern, Switzerland
[b)] Paul-Scherrer-Institute (PSI), 5232 Villigen, Switzerland

Corresponding author: ellina.bernard@geo.unibe.ch

Highlights

- Micro-X-ray diffraction (µ-XRD) is a powerful tool for spatially resolved (2D) phase identification in heterogeneous materials
- µ-XRD measurements result in mineral distribution maps across claystone – concrete interfaces
- In the concrete, ettringite, C-S-H and portlandite (if present) are not observed in layers parallel to the interface
- Calcite precipitates evenly spread in the cement or concentrated at the interface depending on the type of cement used

Keywords

Micro-X-ray diffraction (µ-XRD); Cement/clay Interface; Opalinus Clay; low-pH cement; Portland cement

Abstract

The safety of a geological repository designed for deep storage of nuclear waste rests on the long-lived isolation properties of the geological environment and the engineered barrier system. To study the chemical and physical behaviour of cementitious/clayey interfaces, such interfaces have been collected during repeat sampling campaigns of the CI Experiment (Cement-Clay Interaction Experiment) at the Mont Terri rock laboratory (St. Ursanne, Switzerland, www.mont-terri.ch) over the last decade. This study focuses on the advanced analysis by µ-XRD mapping to locate and identify the mineral phases on each side of the interface. The hydrates as portlandite, ettringite and C-S-H present in the Portland cement (PC) were dissolved in contact with the Opalinus Clay (OPA) up to different depths (~0.2 mm for portlandite; ~1 mm for ettringite; completely depleted for C-S-H up to 0.1 mm and less visible on a 1-mm-depth) while the ettringite from ESDRED (a low-pH cement type) seems to be destabilized to a larger depth ($\geqslant$3 mm). In contrast to former studies, calcite could not be clearly observed at the interface PC - OPA but was well developed at the interface ESDRED - OPA. The extent of reaction after 10 years is very small in both cases, and dissolution of clay minerals remains below detection. The identification of mineral phases involved in reactions facilitates the understanding of the processes, thus, will help to improve the reactive transport models used to simulate the evolution over long times.

1. Introduction

Clay-rich rocks currently under consideration for host rock at an advanced stage of repository planning include Opalinus Clay (OPA) in Switzerland (NAGRA, 2002), Callovo-Oxfordian "argillite" in France (ANDRA, 2005), and Boom Clay in Belgium (SCK • CEN, 2012). Clay-based geological barriers have low permeability and high

sorption capacity which limits the ingress of groundwater and mobility of most radionuclides and are thus favourable to contain radioactive residues (ANDRA, 2005; NAGRA, 2002; SCK • CEN, 2012).

The pH values in the porewater can reach 13.5 in freshly hydrated Portland cement (PC) due to the high alkali content in such solutions (Berner, 1992; Lothenbach and Winnefeld, 2006; Vollpracht et al., 2015). This is likely to impact claystone and swelling clays at the contact zone as summarized e.g. in (Gaucher and Blanc, 2006; Savage et al., 2007). The combination of high pH values and alkali concentrations leads to the partial dissolution of clayey rocks (Adler et al., 1999; Claret et al., 2002) or geotechnical clays / bentonites (Bauer and Berger, 1998; Ramírez et al., 2002) with the formation of calcium aluminate silicate hydrate phases and zeolites; zeolite formation is favoured at increased temperature (Fernández et al., 2010; Lalan et al., 2016; Lothenbach et al., 2017). To lower the impact of an alkaline plume disturbance of the swelling clay, so-called "low-pH" binders have been developed, which contain in addition to PC, pozzolanic materials such as silica fume, fly ash or slag (Cau Dit Coumes et al., 2006; Codina et al., 2008; Lothenbach et al., 2012; Lothenbach et al., 2014). The hydration products of such low pH- cement pastes are mainly calcium silicate hydrate (C-S-H) and ettringite, while portlandite is generally absent. The presence of pozzolanic materials which react with the portlandite, lowers the pH values of the pore solution; pH values in the range from 11 to 12 (Bach et al., 2013; Cau Dit Coumes et al., 2006; Codina et al., 2008; Lothenbach et al., 2012; Lothenbach et al., 2014) have been observed for "low-pH" cement pastes after 3 months of hydration. The presence of silica-rich materials lowers the Ca/Si ratio in C-S-H to 0.7-1.2, compared to approx. 1.9 in PC pastes.

The Cement–Clay Interaction (CI) Experiment carried out at the Mont Terri rock laboratory in Switzerland aims at reducing uncertainties in the process understanding of cement-clay interaction; details can be found in (Mäder et al., 2017). A time frame

of at least 20 years is foreseen for the CI experiment, which was installed in 2007. Sampling campaigns were carried out in 2009, 2012, 2015, 2017, and 2018. Cementitious materials include PC concrete and two types of low-pH concretes (blend of PC and silica fume, so-called ESDRED, a low alkali slag cement so-called LAC). Also emplaced was a layer of bentonite that was artificially saturated over the first year of the experiment.

In this study, the focus is made on interface samples between OPA and two different types of cementitious materials, either a PC paste or a low-pH cement paste (ESDRED).

Results of sample analysis from interfaces between the different concretes (PC and low-pH slag cement + aggregates) and OPA were presented in detail by (Jenni et al., 2014) and (Mäder et al., 2017), while (Dauzères et al., 2016) and (Lerouge et al., 2017) put the focus on the concrete part and Mg–Si-hydrates. (Mäder et al., 2017) summarized and compared the main findings regarding the chemical, mineralogical, and microstructural changes occurring after relatively long time periods (on 2.2 and 4.9-year-old samples) and under realistic boundary conditions for concretes. Chemical analyses based on SEM/EDS or EPMA, showed that both cements at the interface feature a de-calcification alteration zone and a sulphate-enriched zone, indicating an ingress of the pore water from OPA in the concrete. In the case of the PC concrete, a distinct enrichment of magnesium was observed in the OPA, detached from the interface, at 6-8 mm distance, while the low pH concretes displayed a wider magnesium enriched zone located at the interface.

Those conclusions were made on interfaces between concrete and claystone. The aggregate present posed limits to bulk analytical methods such as powder XRD measurements. For this reason, pastes and mortars of PC and ESDRED cement pastes or mortars were emplaced in 2012, and these were sampled in 2015, specifically for the

purpose of applying alternative analytical techniques such as µ-XRD, but also some isotopic methods on spatially resolved small bulk samples.

This study describes the mineralogical and chemico-physical evolution of reaction zones at the interface between the cement pastes and the OPA and subsequently compares multiple samples from the CI experiment including different paste, mortar and concrete interfaces with OPA. New mineralogical findings allow for an improved and more detailed understanding of interaction processes and support so far speculative mechanisms.

2. Materials and methods

The samples studied correspond to interface Portland cement paste – Opalinus Clay (PC-OPA) and low-pH cement paste – Opalinus Clay (ESDRED-OPA). Binder compositions at the time of the emplacement in 2012 are detailed in the following. The PC paste contains 1260 kg/m^3 cement (CEM I 42.5N) with a water to binder ratio (w/b) equal to 0.47, and the low-pH cement paste 653 kg/m^3 cement (CEM I 42.5N), 438 kg/m^3 silica fume (SikaFume HR7) with a w/b=0.50 (containing superplasticizer and accelerator). The mortar compositions are described in the supplementary information, concrete formulations are given in (Jenni et al., 2014). The paste and mortar interfaces have been sampled in 2015 after 3.2 y of interaction, the concrete interfaces sampled in 2017 after 10.2 y of interaction.

2.1. Sample preparation

Polished sections of the interface between hydrated pastes and OPA were prepared as detailed in (Mäder et al., 2017), avoiding, on one hand, the rehydration of remaining clinker phases in the cement or changes in cement hydrate element repartitions, and, on the other hand, the swelling/shrinkage of clay minerals and pyrite oxidation in OPA.

To obtain thin sections appropriate for µ-XRD work, similar precautions were followed. The surface of rectangular samples were glued onto a 200 µm thick optically pure SiO_2-glass coverslip (dimensions: 22/22/0.20 mm, quality: HER102 (Herasil® 102 from Heraeus), Ident-Nr.: 09601003, www.wisag.ch) (Figure 1). Then, this SiO_2-glass slip was glued onto a regular thin section support glass. The interface sample was ground and polished to ~30 µm thickness with kerosene lubricant and diamond pastes and cleaned with hexane. Next, the polished sample surface was glued onto a rectangular support glass with a circular through-hole of ~1 cm diameter, centred with the sample region of interest. Finally, the support glass was ground off, and the 200 µm thick pure SiO_2-glass slip was polished down to a thickness of ~50 µm.

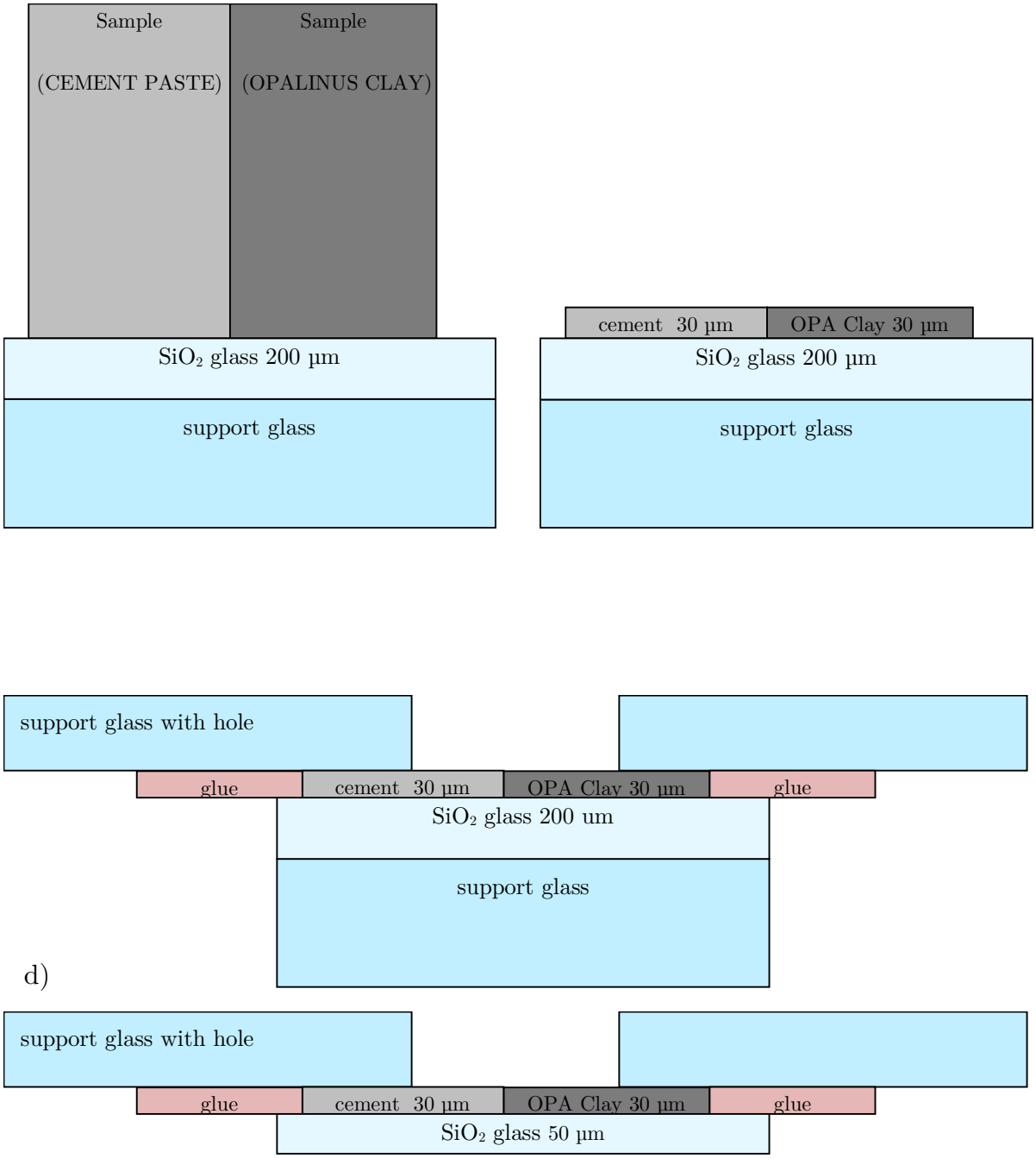

Figure 1: a) initial step of the thin section preparation. The block cut from the drill core is glued onto a 200 µm SiO_2-glass slip, which is again glued onto a standard glass slide for increased mechanical stability during sample handling; b) the sample is cut, ground and polished to a thin section of ca. 30 µm thickness; c) the support glass with hole is glued onto the thin section. This standard glass slide has a hole of ca. 1 cm diameter allowing for direct X-ray beam access to the area of interest and can be attached to the beamline sample holder; d) the final sample. The lower support glass is completely ground away and the pure quartz glass slide ground to ca. 50 µm. The final ratio of sample to glass support is ca. 1:2.

2.2. Analytical techniques

2.2.1. SEM/EDS

Thin sections and polished sections of interface samples were examined by SEM/EDS. The uncoated sample surfaces were examined in a scanning electron microscope (SEM, Zeiss EVO-50 XVP) equipped with an EDAX Sapphire light element detector in low vacuum mode (10 Pa) with a beam acceleration of 20 kV and a working distance of 9 mm. The beam current was adjusted to yield a dead time of 10-20%. Element dispersive X-ray spectroscopy (EDS) maps with 512x400 pixels were acquired using a dwell time of 300 µs and 32 or 64 averaged frames. Multiple maps were combined to cover the area of interest, requiring total measurement times of 8-12 h for each section. Typically, the overall map is composed of 15 to 25 columns and 2 to 4 rows. Higher resolution (1024x800 pixels), but lower dwell times were used to acquire backscatter electron (BE) images, which depict the average proton number at beam location. Brightness and contrast of the maps were adjusted to reveal gradients within cement or clay matrix, often resulting in over- or under-saturation (in grey-scale) of phases of no interest. Exploring precision of the SEM stage movement, electron beam stability, and image distortion, BE images and smaller maps (higher resolution) were also acquired and assembled.

Multiple EDS maps have been acquired in a grid with columns parallel to the interface and rows perpendicular to it. During the acquisition of each map, the EDS detector collected X-rays from the entire map area. The resulting spectra of each map were quantified standardless using a ZAF correction. The quantifications of each column of maps parallel to the interface were averaged as in (Jenni et al., 2017). The averages were plotted as a function of the distance from the interface (chemical profiles across the interface); the range of the different element map quantifications in one column indicates the chemical variability parallel to the interface and this is plotted as bars in the figures.

Additionally, smaller hand-picked area measurements across the interface were measured every 50 µm in the cement or clay matrix, avoiding any larger grains (e.g., quartz, calcite, dolomite, pyrite) to obtain better resolved chemical profiles. The low- and high-resolution profiles agree well in general. The large averaged maps show a higher content of calcium, sulphur or iron due to large calcitic bioclasts and pyrite nests heterogeneously distributed, as detailed in (Jenni et al., 2017), which were not measured in the hand-picked area measurements. Data of averaged element maps from mortar or concrete cannot be used due to the large aggregates, filling random fractions of each map. Acquisition of even larger maps would solve this issue, but at the expense of too small a spatial resolution, considering the thinly layered chemical heterogeneities in the matrix.

In both standardless quantification approaches, the sum of all elements present is normalised to 100%, except the elements too light for quantification (H, O, C). Therefore, an absolute decrease of one element is compensated by an increase of all other elements (e.g., porosity, mostly filled by the organic resin, is not part of the quantification).

2.2.2. Relative µ-XRD maps and XRD profiles

Detailed spatially resolved µ-XRD measurements were performed at the Swiss Light Source (SLS). The X05LA microXAS Beamline used is especially designed for µ-beam X-ray analyses. A thin section (30 µm thickness) perpendicular to the interface containing up to 3 mm of OPA and cement paste was prepared as detailed above. The sample was mounted vertically onto an X-Y-Z-rotation stage. The rotation axis is perpendicular to the beam, in order to be able to rotate the sample for measuring different crystal orientations (rocking of +-20° perpendicular to the beam during the dwell time). The beam (9.700 keV energy, 1.2782 Å wavelength) was focused to a spot

size of either approx. 5 or 25 µm on the sample and the distance of the sample to the detector was ca. 5.2 cm. A 2D XRD pattern was measured at each position within the region of interest with a dwell time of 5 s. The resolution of the resulting maps (equal to the step size of stage movement) was 10 µm for measurements with the 5 µm beam, and 25 µm for the 25 µm beam.

This improved acquisition allowed for continuous measurement during rotation, in contrast to the acquisition of multiple frames at defined rotation angles as done previously (methodology further discussed in the supplementary material). Several regions across the interface and further away have been mapped.

During the data treatment, the resulting 2D frame of each point of the µXRD map were integrated to 1D diffraction pattern. The counts of the main peaks of a specific mineral were used to generate phase distribution maps with the XRDua software (De Nolf et al., 2014), (www.xrdua.ua.ac.be). Then, the maps of the characteristic reflections for one specific mineral were averaged. The resulting mineral map shows the relative spatial distribution of one mineral, and gives no indications of its amount. Furthermore, large single crystal grains (e.g., alite) might, despite sample rocking, never fulfil Bragg's equation and might not be visible on the mineral map. More details are given in the supplementary material.

Interface samples from the same campaign (pastes or mortars) were used to obtain conventional XRD powder-like patterns as a function of distance from the interface. An approximately 4 cm cube containing the interface was ground parallel to the interfacial plane to expose surfaces at different distances to be analysed. Diffraction data were collected on each surface with a PANalytical X'Pert Pro MPD diffractometer, equipped with a Cu X-ray source and an X'Celerator detector, from 4 to 70° 2θ with a total integration time of 80 s per step. Automatic divergence slits (9 mm irradiated length) and 0.02 radian Soller slits were used. Prior to qualitative data

evaluation, all diffraction patterns were converted to "fixed slit" data with PANalytical HighScore Plus v. 4.6.1.

3. Results and discussion

We focus in this part on the results obtained on PC paste (section 3.1) and ESDRED cement paste (section 3.2) in contact with OPA collected after 3.2 years. The samples were first investigated by SEM/EDS to trace the chemical changes. The geometry of the observed zones of different chemistry provides the basis for the more complex and time-consuming µ-XRD maps at specific locations. Conventional XRD and semi-quantitative mineral distribution maps (Rietveld refinement approach presented in supplementary material) obtained on similar interfaces but with mortars in contact with OPA are used for comparison.

3.1. Interaction of Portland cement and Opalinus Clay

3.1.1. Chemical changes at the interface

Semi-quantitative profiles of the EDS elements across the interface (Figure 2a and b) and EDS maps of calcium, magnesium, sodium, silicon and aluminium element (Figure 2c), taken on a 3.2-year-old paste sample, reveal the following zoning patterns. The cement paste at the interface contained less calcium (45 mol% compared to 55 mol% in the unaltered cement paste), while slight increases of silicon (from 22 mol% to 32 mol%), aluminium (from 7 mol% to 12 mol%) and sulphur (from 2 mol% to 4 mol%) were observed. The calcium maps (Figure 2c and Figure 3) reveal a distinctly darker zone (less calcium) at the very interface, but no brighter aluminium zone (more aluminium) in the corresponding map. Therefore, the aluminium increase seen in spot measurements (Figure 2a) is interpreted as a relative increase due to normalisation (but constant amount of aluminium per volume), compensating a volumetric calcium decrease and corresponding increase in porosity (not measured). In contrast, the increase in sulphur and sodium, and probably also in silicon, is too strong to be only

a compensation effect. Comparable SEM/EDS and EPMA results were already observed in younger and older samples on a comparable interface (Mäder et al., 2017). Similarly, the magnesium content (4 mol%) is relatively homogeneous in the cement paste at the interface, but it is higher in the OPA at a distance of 2-3 mm from the interface (very edge in Figure 2c). The oblique (compared to trace of interface) high-magnesium zone in Figure 2c leads to a large variability in data projected parallel to the interface (large bar in Figure 2, left-most measurement in OPA). This magnesium-enriched zone in the claystone-side was better observed at 6–8 mm distance in the concretes samples aged of 4.9 years by EPMA (Mäder et al., 2017). The present magnesium enrichment observed at the very edge (arrow in Figure 2c) could be deeper in the OPA and/or the premises of a larger magnesium enrichment occurring after longer time.

The high-silicon grains in the cement are associated with residual quartz grains, probably trace components from the clinker or grains incorporated during emplacement but not formed in-situ.

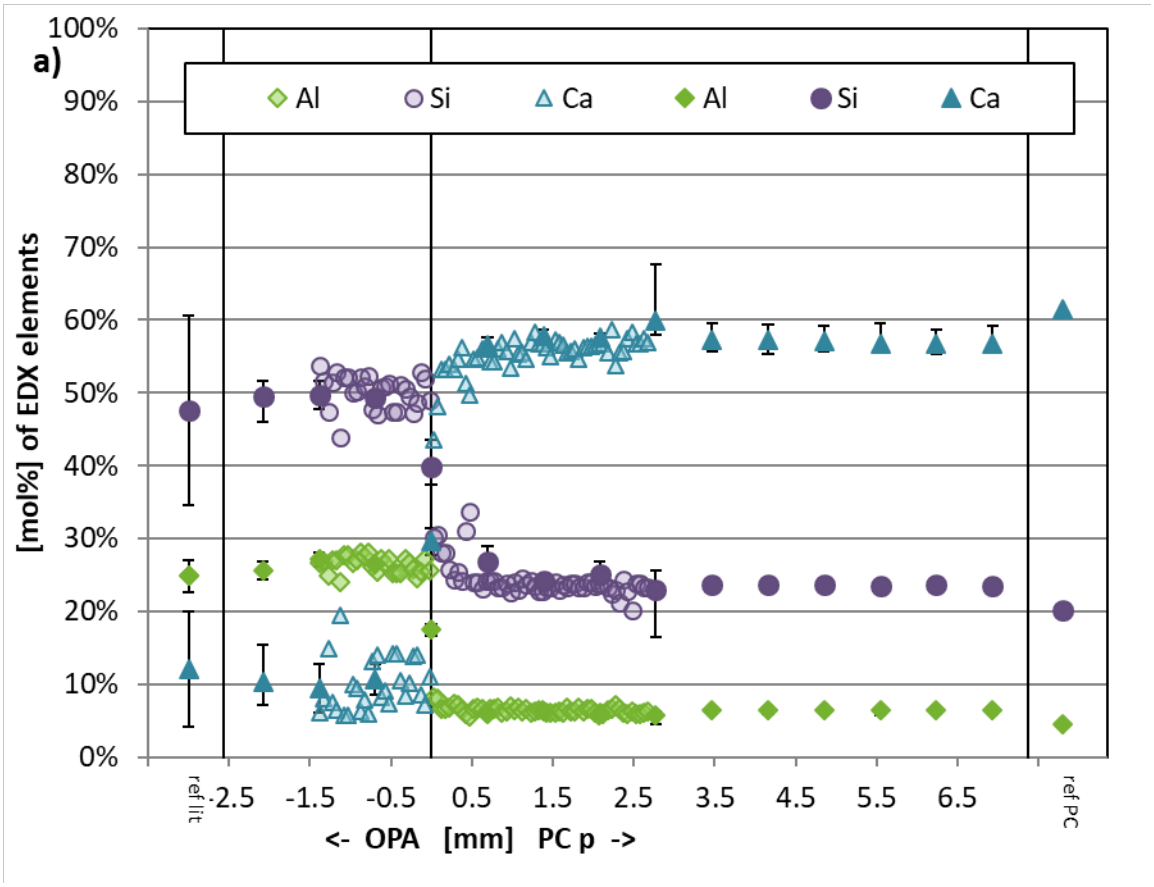
a)
Al
Si
Ca
Al
Si
Ca
100%
90%
80%
70%
60%
50%
40%
30%
20%
10%
0%
[mol%] of EDX elements
ref lit
-2.5
-1.5
-0.5
0.5
1.5
2.5
3.5
4.5
5.5
6.5
ref PC
<- OPA [mm] PC p ->
b)
Na
Mg
S
K
Na
Mg
S
K
10%
9%
8%
7%
6%
5%
4%
3%
2%
1%
0%
[mol%] of EDX elements
ref lit
-2.5
-1.5
-0.5
0.5
1.5
2.5
3.5
4.5
5.5
6.5
ref PC
<- OPA [mm] PC p ->

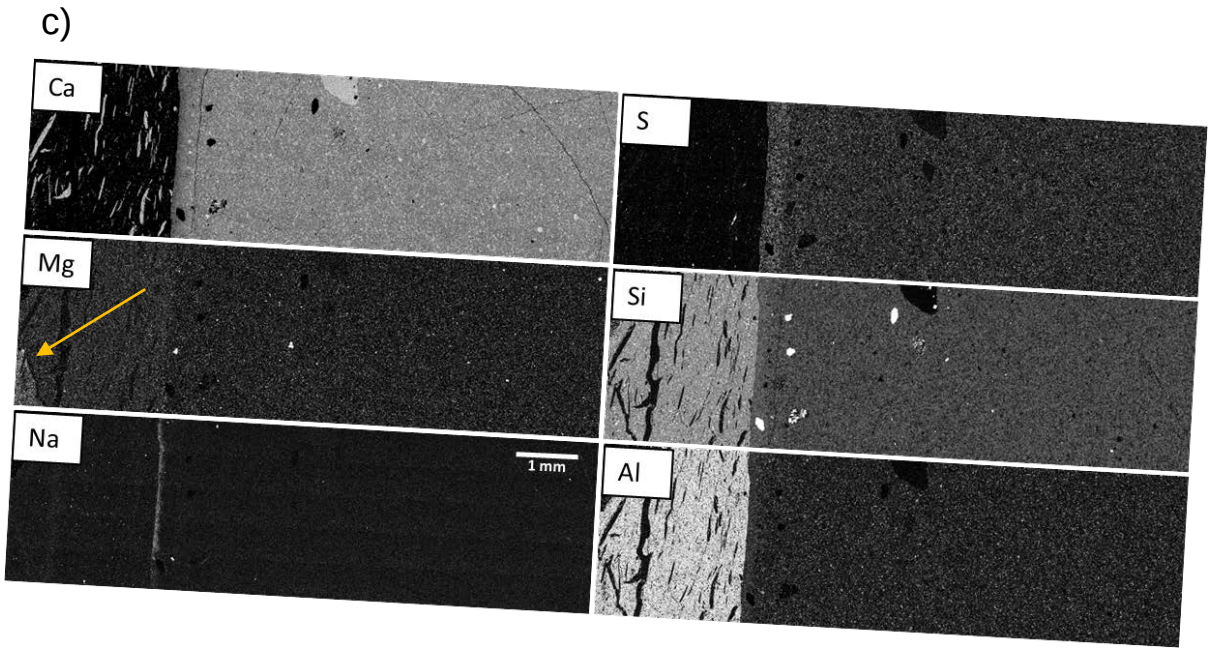

Figure 2: a) and b) Profiles determined by EDS across the interface Portland cement paste (PC p) - Opalinus Clay (OPA) after 3.2 years. Filled symbols with bars show the average chemistry of an area map (see chapter 2.2.1) while the shaded symbols correspond to area measurements chosen by hand in the homogeneous matrix close to the interface (Cl is approximately constant at 1 mol%). Reference values of undisturbed state are shown at left and at right, either measured (PC) or from literature (OPA); c) EDS element maps across the Portland cement paste - Opalinus Clay interface after 3.2 years.

3.1.2. Crystallography and solid phases

The main goal of this study is to link the chemical changes observed previously (Dauzères et al., 2016; Jenni et al., 2017; Jenni et al., 2014; Lerouge et al., 2017; Mäder et al., 2017) to the dissolution and precipitation of minerals. An overview (Figure 3) of the different areas where the µ-XRD and EDS data (detailed in the section above) were recorded also displays some shrinkage cracks due to drying. They have been filled with resin during impregnation along with macropores (black in Figure 3). The different areas mapped with µ-XRD include the interface (2 different resolutions, XRD1 and XRD2), OPA away from the interface (XRD3), and across the interface extending far into the PC paste (XRD4). In the OPA, high-calcium areas in the EDS map correspond to high-calcite areas in the µ-XRD maps (mainly calcitic bioclasts).

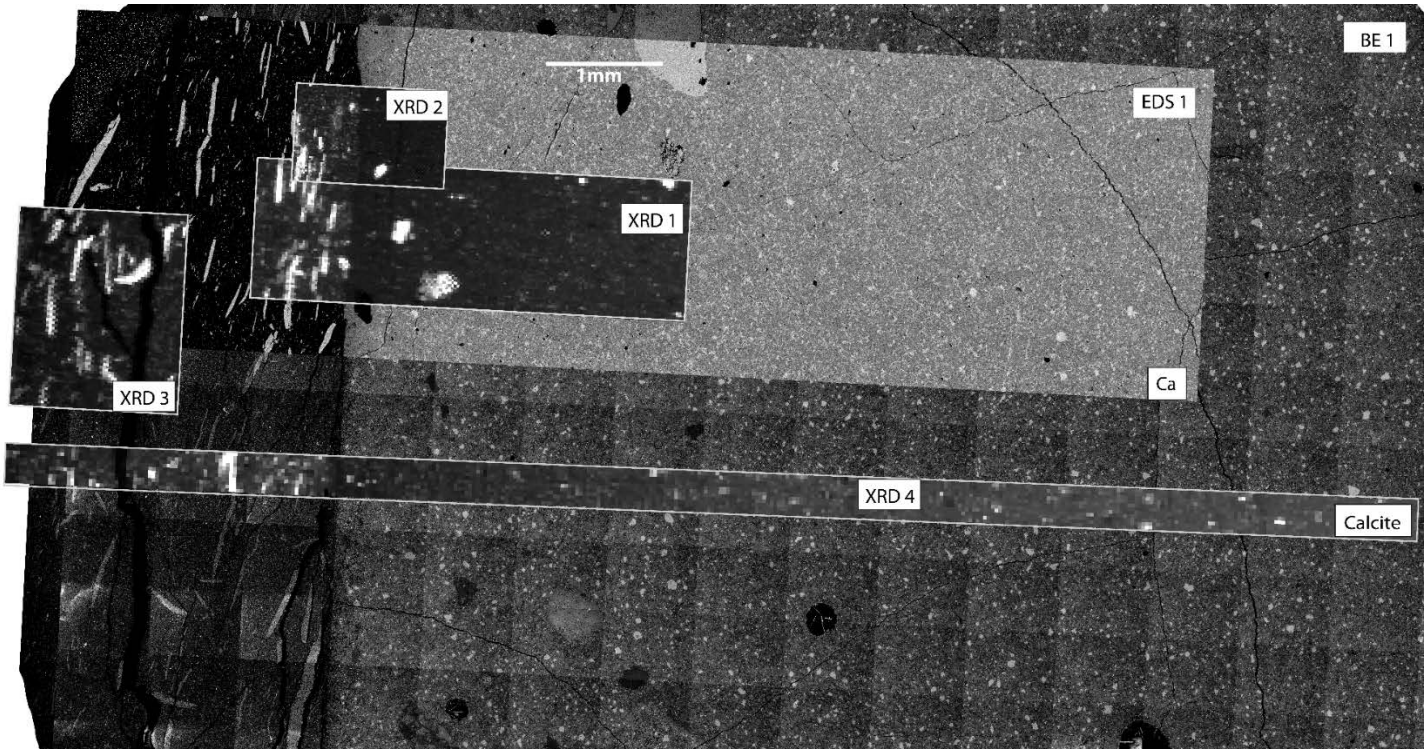

Figure 3: BE background, EDS-calcium element map and Calcite μ-XRD maps of the Portland cement paste-Opalinus Clay interface after 3.2 years.

3.1.2.1. Hydration of cement paste

The SEM backscattered electrons images (Figure 3) showed a lower content of unhydrated clinker close to the interface. To quantify this amount relative to the content found in the unaltered paste, the images were processed and the relative content of unhydrated clinker (content of unhydrated clinker/average of the unhydrated clinker far from the interface) was plotted versus the distance from the interface (Figure 4a). Its content was 20% lower in the first millimetre in contact with the OPA.

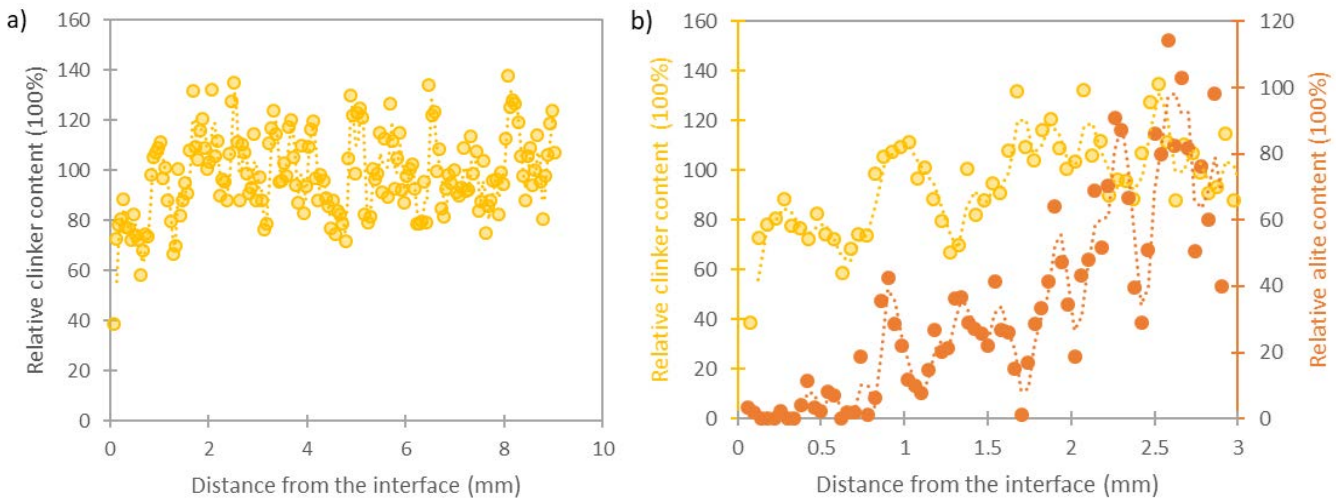

Figure 4: a) Clinker content quantified from the BE images expressed as (clinker content)/(clinker content average in the unaltered Portland cement paste) versus the distance from the interface; b) same clinker content compared to alite content quantified from the μ-XRD map, expressed as (alite content)/(alite content average in the unaltered Portland cement paste) versus the distance from the interface.

Alite (C_3S) could be detected by μ-XRD analysis and its relative intensity mapped (Figure 5a), and after image processing, a profile from the interface to the unaffected paste plotted (Figure 4b). Although alite was not observed at the interface by μ-XRD analysis, it doesn't indicate that its content is reduced to zero (see section 2.2.2). The lower content of alite close to the interface confirms a higher hydration degree of the paste close to the interface compared to further away from the interface.

With ongoing cement hydration and resultant water shortage, OPA pore water is expected to enter the cement (hydraulic gradient and capillary forces). The continuously penetrating solution with a neutral pH pushes the additional hydration of alite and belite, i.e. their dissolution and precipitation of hydrates. Also, the pore solution of OPA contains sulphate (1-2 g/l) and this would favour the hydration of aluminate (C_3A) and ferrite (C_4AF) to form ettringite (AFt phase) and monosulphoaluminate, monocarboaluminate and others (AFm phases) (Matschei et al., 2007).

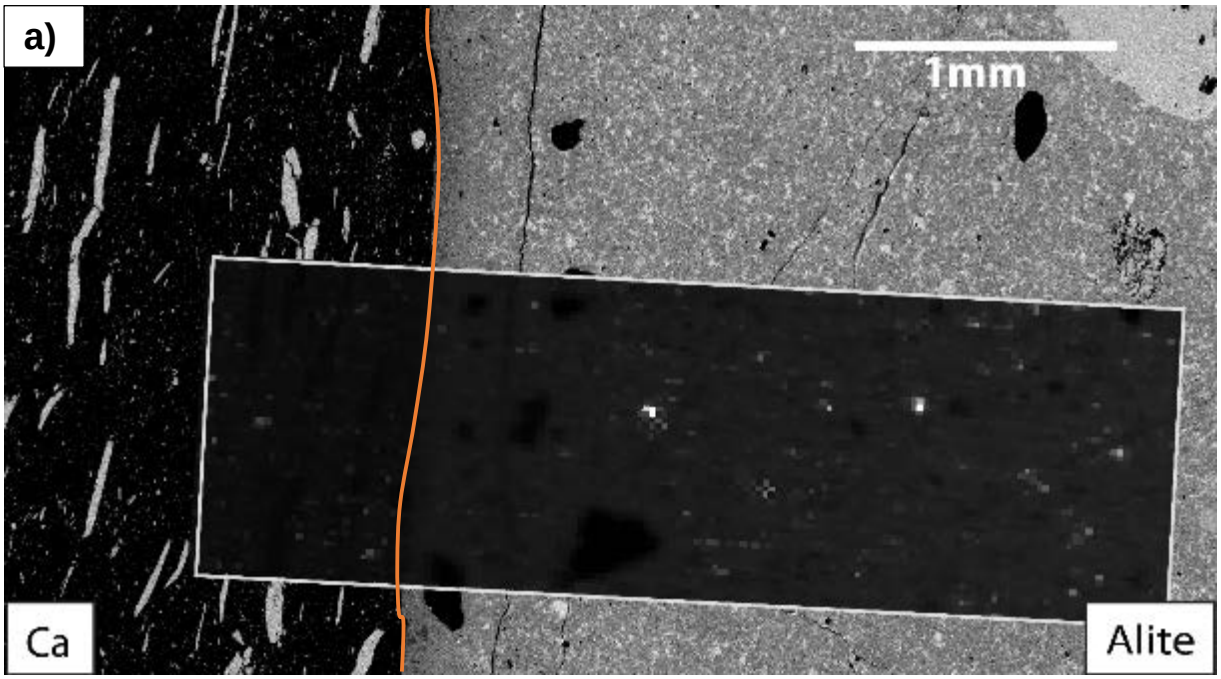
a)
1mm
Ca
Alite

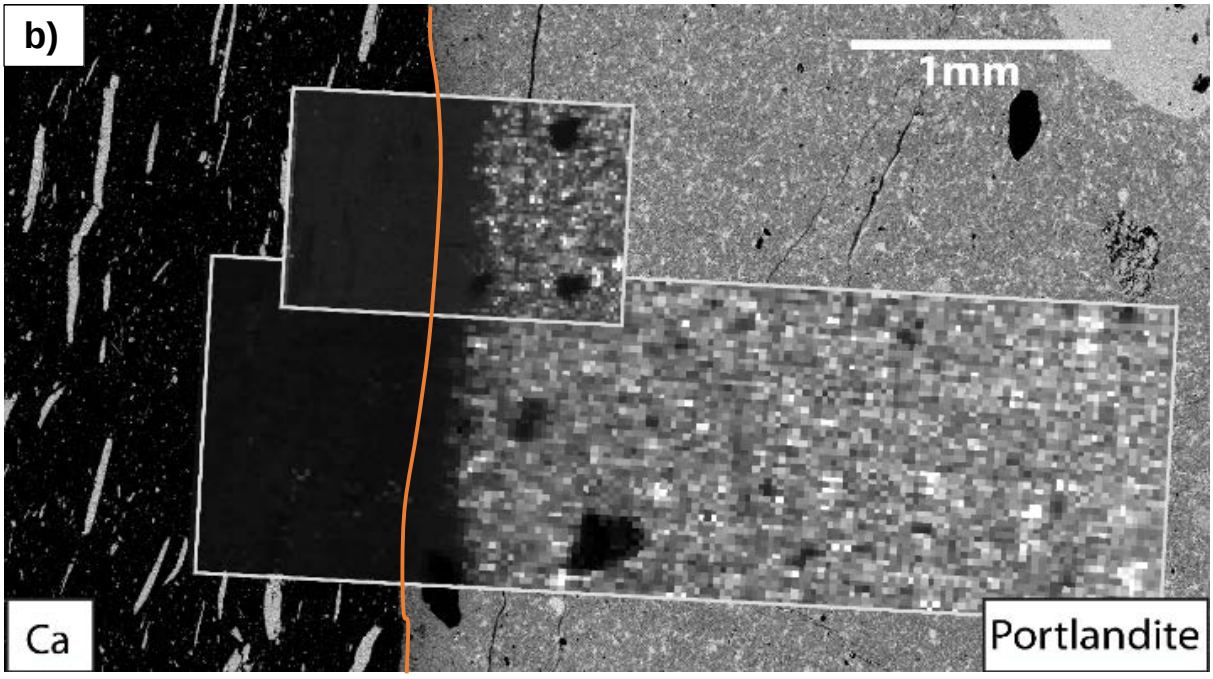
b)
1mm
Ca
Portlandite

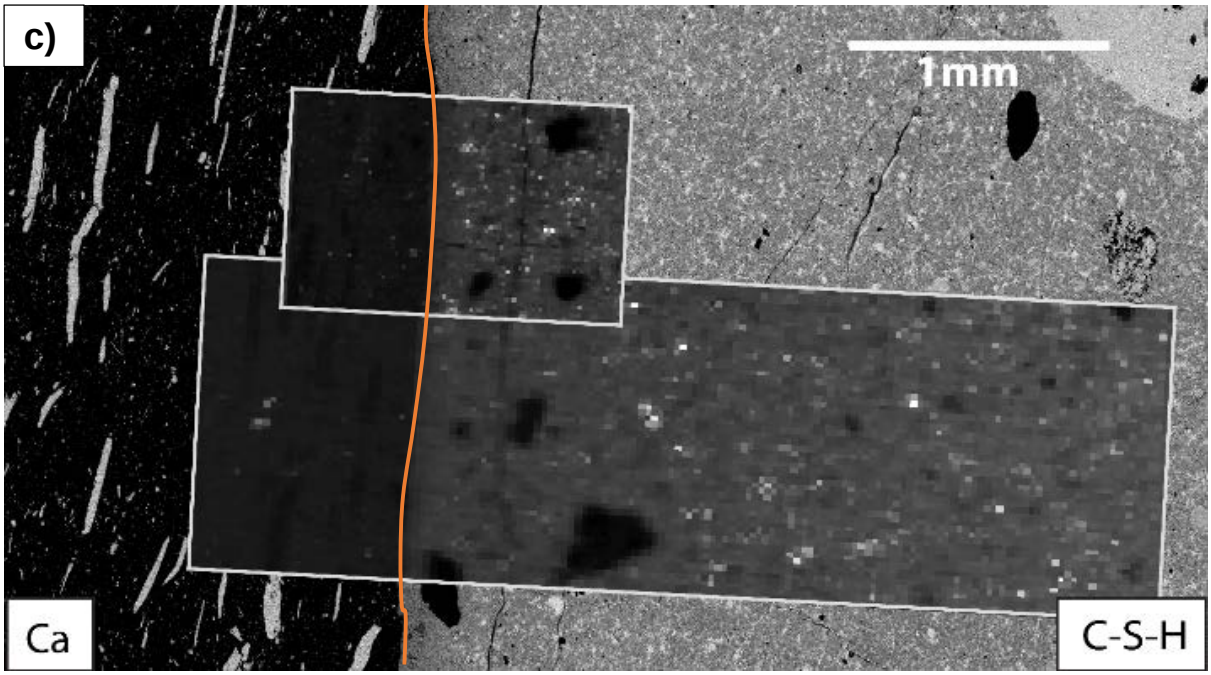
c)
1mm
Ca
C-S-H

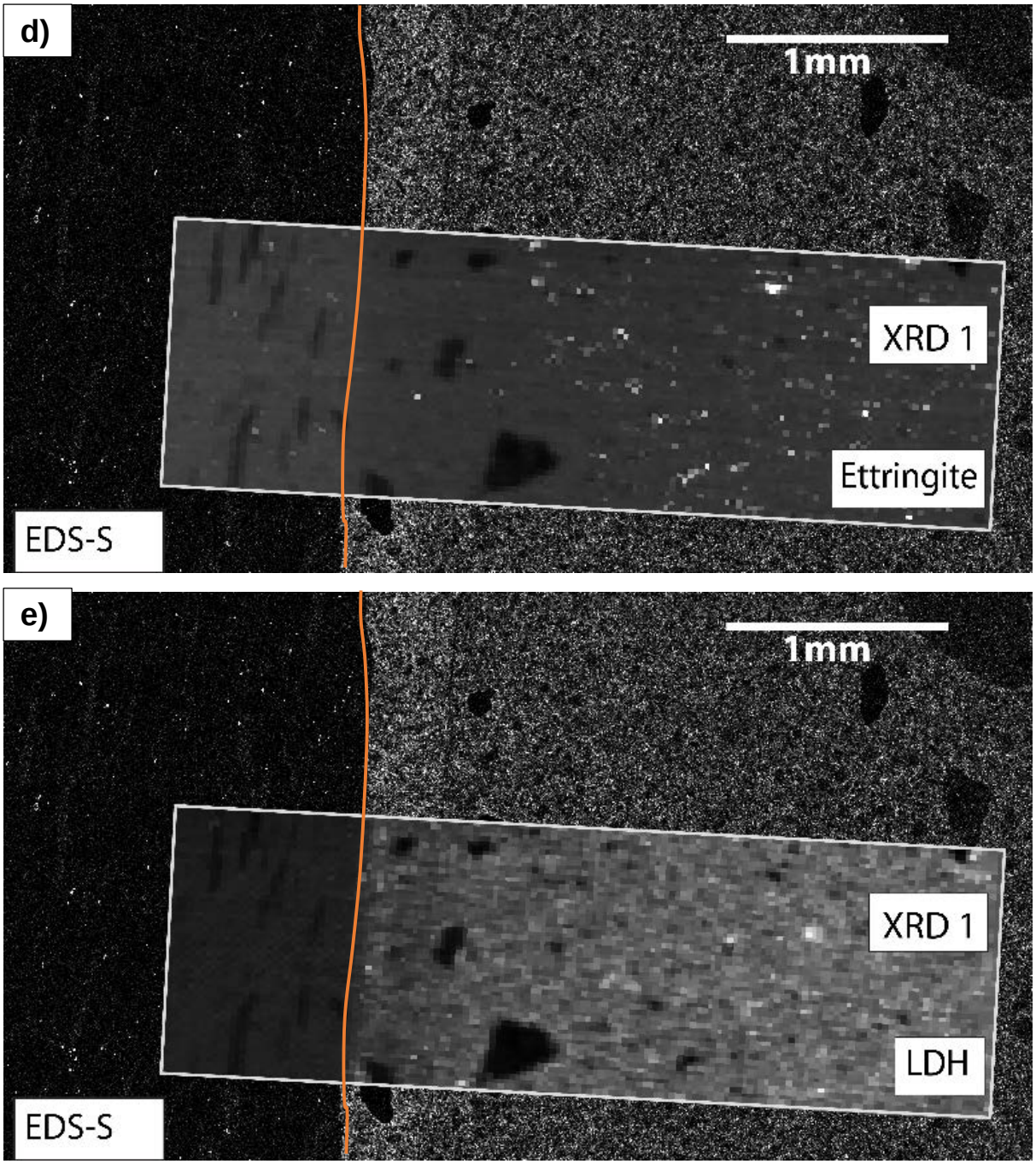

Figure 5: SEM/EDS-calcium element map and μ-XRD intensity distribution map of a) alite, b) portlandite and c) C-S-H, SEM/EDS-sulphur element and μ-XRD intensity distribution map of d) ettringite and e) LDH-like phase (top: 5μm-beam size bottom: 25μm-beam size);the orange line indicates the interface between Opalinus Clay (left) and Portland cement paste (right), aged of 3.2 years.

3.1.2.2. Faith of calcium

Portlandite and C-S-H

The bulk XRD patterns (Figure 6) acquired on surfaces of the mortar sample at different distances from the OPA showed lower intensities of portlandite reflections close to the OPA. Ettringite was absent at the interface but detected starting at 0.3 mm distance. The dissolution of portlandite and/or ettringite is expected with a decrease of pH induced by the contact with the OPA.

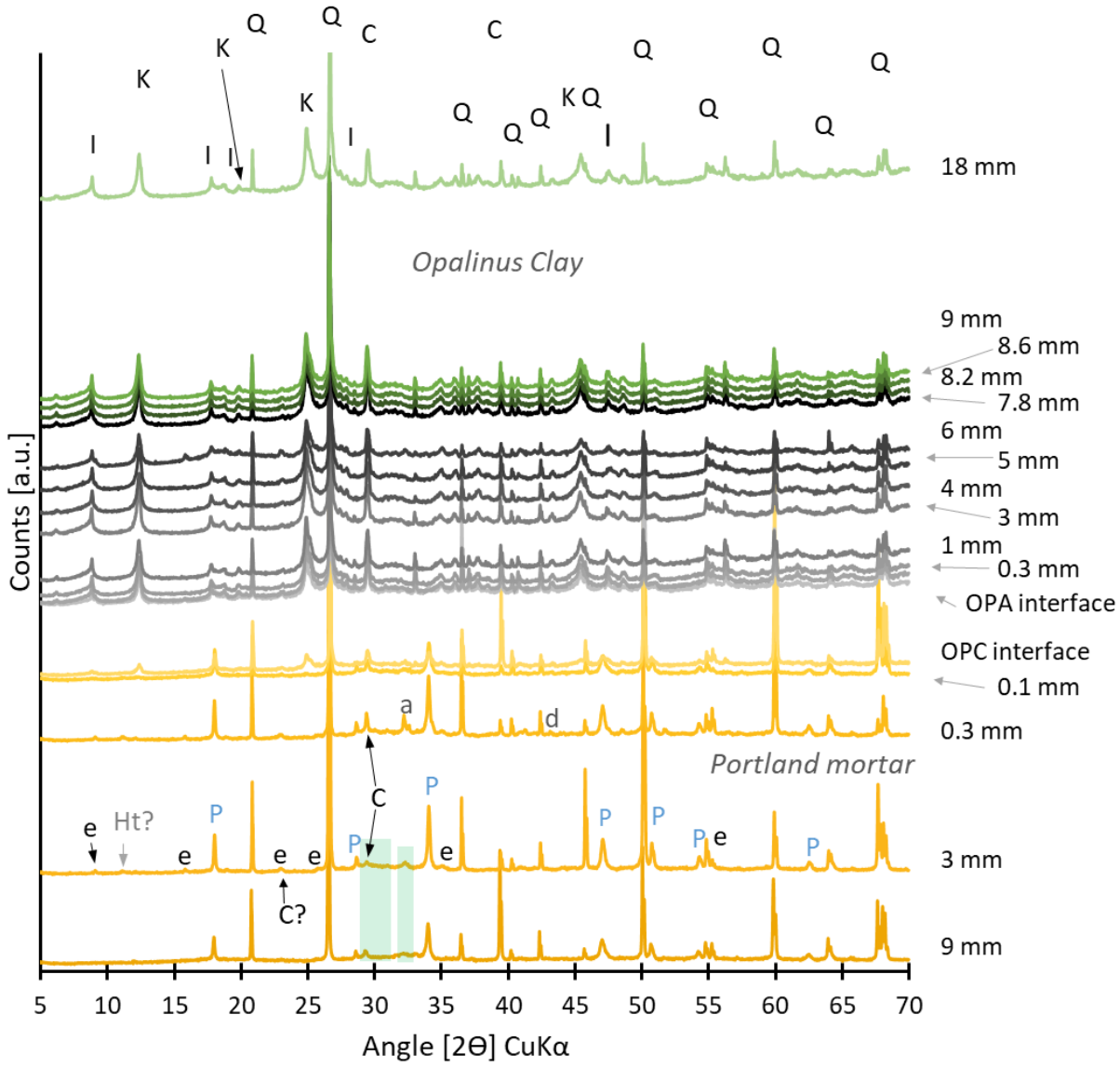

Figure 6: X-ray diffraction patterns of sequentially ground surfaces in Opalinus Clay and Portland cement mortar at different distances from the interface. Sample collected from a 3.2-year-old interface. C=calcite, Q=quartz, I=illite, K=kaolinite, e=ettringite, Ht=hydrotalcite, P=portlandite, a=alite, d=dolomite.

Portlandite was observed by µ-XRD within the first 0.2 ± 0.05 mm cement zone in contact with OPA in multiple samples and independent of the beam size chosen for the µ-XRD maps (Figure 5b). Similarly, Portlandite was only observed in the mortar sample away from the interface and quantified around 40 wt. % in the sound mortar (supplementary material). This portlandite-depleted zone coincides with a low-calcium zone in the EDS map. The dissolution of portlandite also explains the depletion of calcium observed up to 0.3 mm on interfaces between PC concrete and OPA: one with a lower w/b aged for 2.2 years and the other one with a similar w/b aged for 4.9 years (Mäder et al., 2017).

The dissolution of portlandite was easily observed due to its high degree of crystallinity while the nano-crystallinity of C-S-H gel (Allen et al., 2007; Haas, 2012; Skinner et al., 2010) results in broad reflection peaks with low intensity. C-S-H was not detected at the interface by conventional XRD due to the large calcite content and peak overlapping. However, it was possible to observe C-S-H by µ-XRD mapping (Figure 5c). The observation is less clear than for well crystalline portlandite, but the content of C-S-H is lower within 0.1 mm from the interface (small beam-size map) and more generally within almost 1 mm from the interface (larger beam-size map). µ-XRD is more suitable to detect C-S-H than conventional XRD where C-S-H might be present away from the interface but facing an overlap with one of the main calcite peaks where both are present. The C-S-H was quantified around 30 wt.% of the sound mortar while its content was negligible at the interface (supplementary material).

The dissolutions of portlandite, ettringite and C-S-H are a known degradation of PC pastes in contact with groundwater, rainwater and seawater over years (De Weerdt and Justnes, 2015; Nishikawa et al., 1992). In contact with the environment, the alkalis and calcium are leached and the pH decrease leads to a destabilization of portlandite

for pH values lower than 12. In our case, it has been suggested that calcium is preferentially taken up in the OPA on the exchangeable cation sites, releasing sodium. The calcium map at this interface (Figure 2) shows slightly increased calcium in the OPA at the interface compared with the OPA reference, while the sodium content might be slightly lower than the one measured in the reference. Increased calcium in OPA at the interface has been observed in various other samples from the Mont-Terri laboratory (Jenni et al., 2014; Mäder et al., 2017).

During a second stage (10.5-11 ≤ pH ≤ 12-12.5), calcium is leached from ettringite and C-S-H, decreasing Ca/Si in the C-S-H until it is destabilized. Ettringite is expected to be unstable for pH below 11 (Jacques et al., 2010) while C-S-H is not stable for pH lower than 9.5-10 (Bernard et al., 2017; Leisinger et al., 2014; Swanton et al., 2016). The absence of ettringite (detailed below) and the presence of C-S-H at the interface indicates pH values at the interface close to or higher than 9.5-10.

Calcite

Calcite is usually formed at the interface, from the decalcification of portlandite and C-S-H and from the in-diffusion of bicarbonate from external pore water (atmospheric or at equilibrium with the OPA pore solution) (see e.g. (Bartier et al., 2013; Jenni et al., 2014; Techer et al., 2012)). However, calcite, or any other crystalline calcium carbonate phase like aragonite or vaterite, were not clearly observed by µ-XRD (Figure 3).

XRD patterns measured directly on the bulk at different distances from the interface in PC mortar collected during the same campaign (Figure 6) indicate the precipitation of calcite. The patterns of the PC mortar directly adjacent to the interface and at 0.1 mm distance contained among other some calcite, illite and kaolinite, indicating the presence of some OPA in the mortar close by. However, the depth of calcite formation in the PC mortar is larger than the perturbation of the analysis by the OPA. Calcite

was observed at 3 mm (without any other OPA phases) but absent further away from the interface (9 mm) indicating a spread carbonation, but still, close to the interface.

Different behaviours of precipitation of calcite between pastes, mortars and concretes from literature are not fully understood. It seems that the paste sample is a particular case compared to the rest of the interfaces. Reactive transport modelling indicates a wide carbonation zone with a low calcite content, where the limiting factor is supply from the OPA pore water and transport across the interface (Jenni et al., 2017). Higher cement porosity leads to lower calcite content over a wider zone that can be seen to extend beyond the extent of the XRD4 calcite map in Figure 3. In line, pastes with similar w/b ratio as mortars or concretes should show higher capillary porosities (Halamickova et al., 1995), which might lead to calcite formation below detection but over a larger volume and a longer distance from the interface. In contrast, calcite is clearly present at the interface in a PC concrete but with a lower w/b (plug cement in Mt Terri CI) at the interface (Jenni et al., 2014).

Ettringite, LDH and faith of sulphate

The µ-XRD maps of ettringite [$Ca_6Al_2(SO_4)_3(OH)_{12} \cdot 26H_2O$] and layered double hydroxide (LDH) structures as monosulphoaluminate, [$Ca_4Al_2(SO_4)(OH)_{12} \cdot 6H_2O$], hydrocalumite or hydrotalcite (Ht or Mg-LDH) are shown in Figure 5d and e. Ettringite was less present at the interface indicating its dissolution. Usually, ettringite is not stable in the presence of Si-Al minerals from the clay and/or carbonated environment (Lothenbach et al., 2017; Nishikawa et al., 1992). However, the dissolution of minerals from the OPA was never observed in former studies of such interfaces, and only minor dissolution was predicted by modelling within the limited interaction time (Jenni et al., 2017). The LDH µ-XRD maps showed a lower content of LDH phases (including AFm and hydrotalcite…) towards the interface. Similarly, hydrocalumite was quantified up to 8 wt.% in the mortar in contact with OPA far from the interface but not observed at the interface (supplementary material). In the

case of the paste, however, a higher content of LDH could be observed very close to the interface. One explanation would be that similarly to ettringite, a lower content of calcium and lower pH values would destabilize the AFm phases close to the interface, while some secondary LDH-like phases would form right at the interface, like poorly ordered hydrotalcite, therefore without calcium.

The EDS sulphur map (Figure 5d or e) or the sulphur profiles (Figure 2) show an accumulation of sulphur in the cement paste at the interface. The sulphate in cement hydrates is known to be taken up by non-silicate mineral phases such as gypsum [$CaSO_4 \cdot 2H_2O$], or precipitation of secondary ettringite (Lothenbach et al., 2010), or possibly in hydrotalcite with a variable Mg/Al ratio (Miyata, 1983). Ettringite was not observed at the interface and the observed sulphate ingress into the cement phase was wider than the possible secondary LDH-like phases that formed at the interface (Figure 5e). The sulphur is thought to be present in C-S-H when still present at the interface. At the very interface, if one only considers the extra sulphur seen in Figure 2c or Figure 5d or e, the S/Si obtained in C-S-H is roughly equal to 0.02-0.05 (mol/mol). These results are higher than the possible adsorption of sulphur onto C-S-H reported in the literature (S/Si ~0.01-0.03 mol/mol; high Ca/Si in C-S-H and elevated temperature favour the sorption) (Barbarulo, 2002).

3.1.2.3. Opalinus Clay and magnesium enrichment

The magnesium-enriched zone, detached from the interface, observed in the OPA (Mäder et al., 2017) and confirmed in this study was investigated by µ-XRD. Chlorite, illite, quartz, brucite and kaolinite µ-XRD maps (Figure 7) compared to the EDS magnesium map show no changes in the mineral proportions at the magnesium enrichment. Crystalline Mg-rich mineral formation such as brucite could not be observed. The magnesium enrichment is 4 times the possible amount of a fully

magnesium-exchanged clay matrix (Mäder et al., 2017) and therefore reflect a newly formed solid phase. The magnesium enrichment seems to be either due to i) a formation of nano-crystalline magnesium silicate hydrated phase (M-S-H) (Nied et al., 2016) (and details below), or ii) a formation of poorly crystalline hydrotalcite (Cavani et al., 1991).

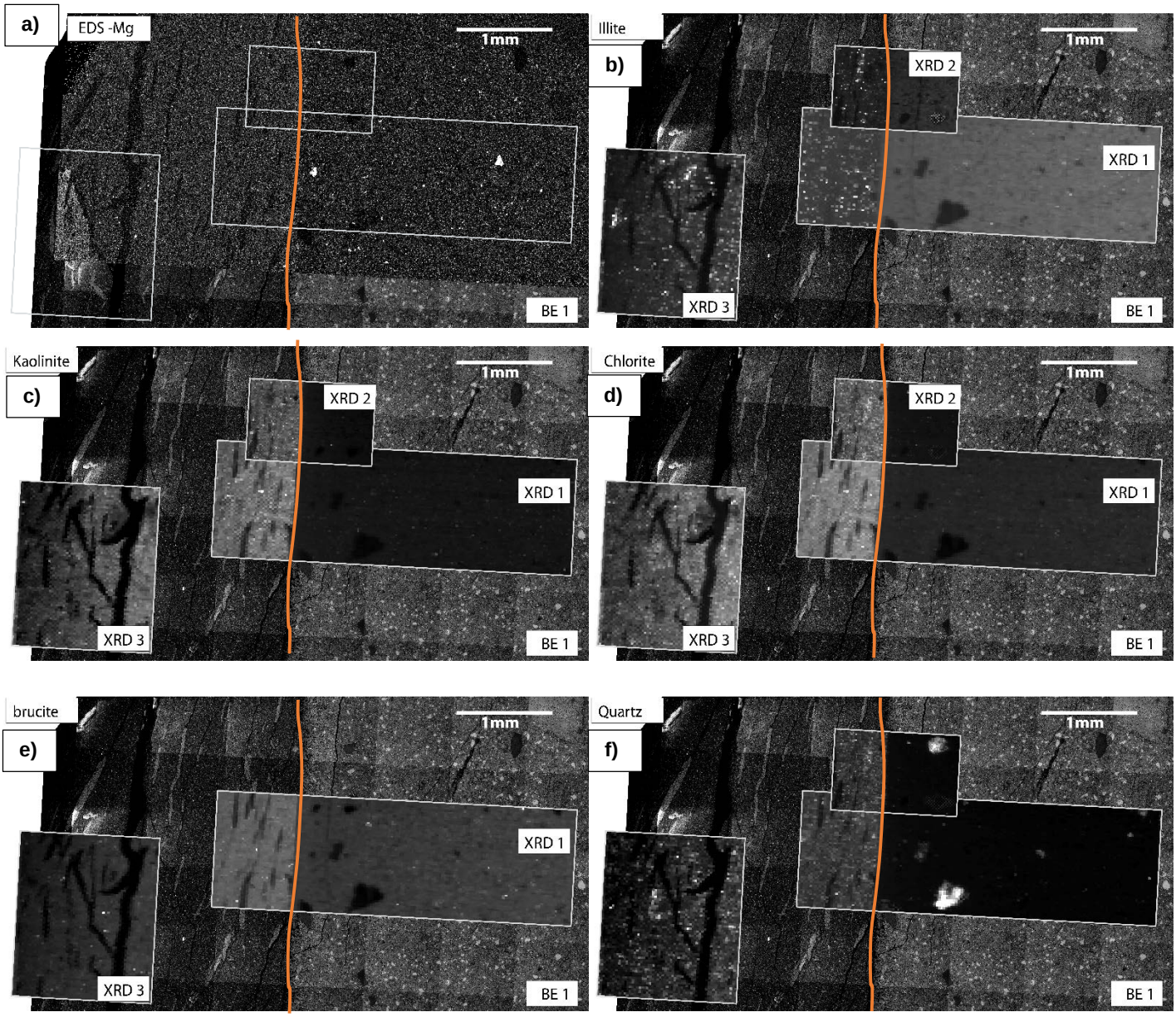

Figure 7: a) SEM/EDS Mg-map and μ-XRD intensity distribution map of b) illite, c) kaolinite, d) chlorite, e) brucite and f) quartz (XRD 1 and XRD 3: 25μm-beam size; XRD 2: 5μm-beam size); the orange line indicates the interface between Opalinus Clay (left) and Portland cement paste (right), aged of 3.2 years.

Investigations of the mortar interface by sliced-XRD also shows no formation of any crystalline Mg-phase. XRD patterns measured at different distances from the interface in each material (Figure 6) show that far from the interface (18 mm) the OPA pattern exhibits characteristic reflections of the major minerals illite (and illite/smectite), kaolinite, calcite, and quartz. The observation of the other minor minerals was obscured and difficult.

Precipitation of magnesium silicate hydrate occurs at a low magnesium concentration (0.01-0.3 mmol/L), a silicon concentration close to amorphous silica solubility and a pH between 8 and 12 (Bernard et al., 2018; Bernard et al., 2017; Bernard et al., 2019b). The formation of nano-crystalline magnesium silicate hydrate in OPA would result from the ingress of hydroxyl ions from the PC paste into the OPA while some minimal dissolution of the clay minerals may occur to buffer the pore solution. Then, the magnesium enrichment might trace the front of the elevated pH zone in the OPA. Reactive transport modelling explains the again lower magnesium content towards the interface by the presence of thermodynamically more favourable hydrotalcite at higher pH (Jenni et al., 2017). The thermodynamic data available associated to OH-hydrotalcite (Lothenbach et al., 2018; Myers et al., 2015) results in very good stabilities in high pH environments (pH $>$ 10.5), although large data uncertainties still exist in the MgO-Al_2O_3-SiO_2-H_2O system.

However, neither M-S-H nor hydrotalcite have been detected by µ-XRD so far and the possible neoformation of magnesium silicate hydrate or hydrotalcite-like phases precipitation in the OPA would need to be experimentally confirmed. The detection of small amounts of very likely nano-crystalline magnesium phases in the multi-mineral OPA is extremely demanding but would provide insight into pH distribution in OPA porewater.

3.2. Interaction of low pH cement and Opalinus Clay

Low pH-cement hydrated pastes are mainly composed of calcium silicate hydrate (C-S-H) and ettringite, while portlandite is absent at expected pH values in the range of 10.5 to <12.5. The addition of nano-silica fume formed clusters in the ESDRED paste withstanding the mixing process, while sand and gravel in mortar and concrete achieved a better dispersion of such clusters.

3.2.1. Chemical changes

Element profiles by EDS (Figure 8) across the interface OPA - ESDRED paste and mortar after 3.2 years, and with ESDRED concrete after 10 years show commonalities but also some differences. The silica fume clusters, sand or aggregate were included in the averaged values of EDS maps (dark symbols with bars), explaining higher values for silicon derived from maps compared to small chosen area analyses of cement matrix (numerous light symbols).

SEM/EDS data show a calcium decrease and a magnesium enrichment in the ESDRED paste at the interface (Figure 13), interpreted in literature as degradation of C-S-H and the formation of M-S-H, respectively, by uptake of magnesium from claystone pore water (Dauzères et al., 2016; Jenni et al., 2014). The magnesium at the interface is particularly enriched in the OPA (Figure 8). These chemical changes occurred in different samples (paste, mortar, concrete) of different ages, to a different extent.

In the case of paste and mortar, an increase of aluminium (from 5 mol% to 8 mol%) and sodium (from 1 mol% to 4.5 mol%) at the interface is seen, while only slight iron (from 1 mol% to 1.5 mol%), sulphur (from 2 mol% to 3.5 mol%) and potassium (from 0.2 mol% to 1.2 mol%) enrichment occurs.

A decrease of chloride is observed in the cement towards the interface, whereas a small sulphur increase is due to normalisation (relatively large decrease in calcium). The initial content of chloride in the ESDRED or in other words, the presence of chloride-

phase in the ESDRED paste compared to the PC might be due to initial presence of chloride in the silica fume used or the migration of chloride from the OPA pore water and its fixation in AFt, or AFm–like phases. The chloride content is below 2%, which makes it virtually impossible to detect a chloride-rich phase.

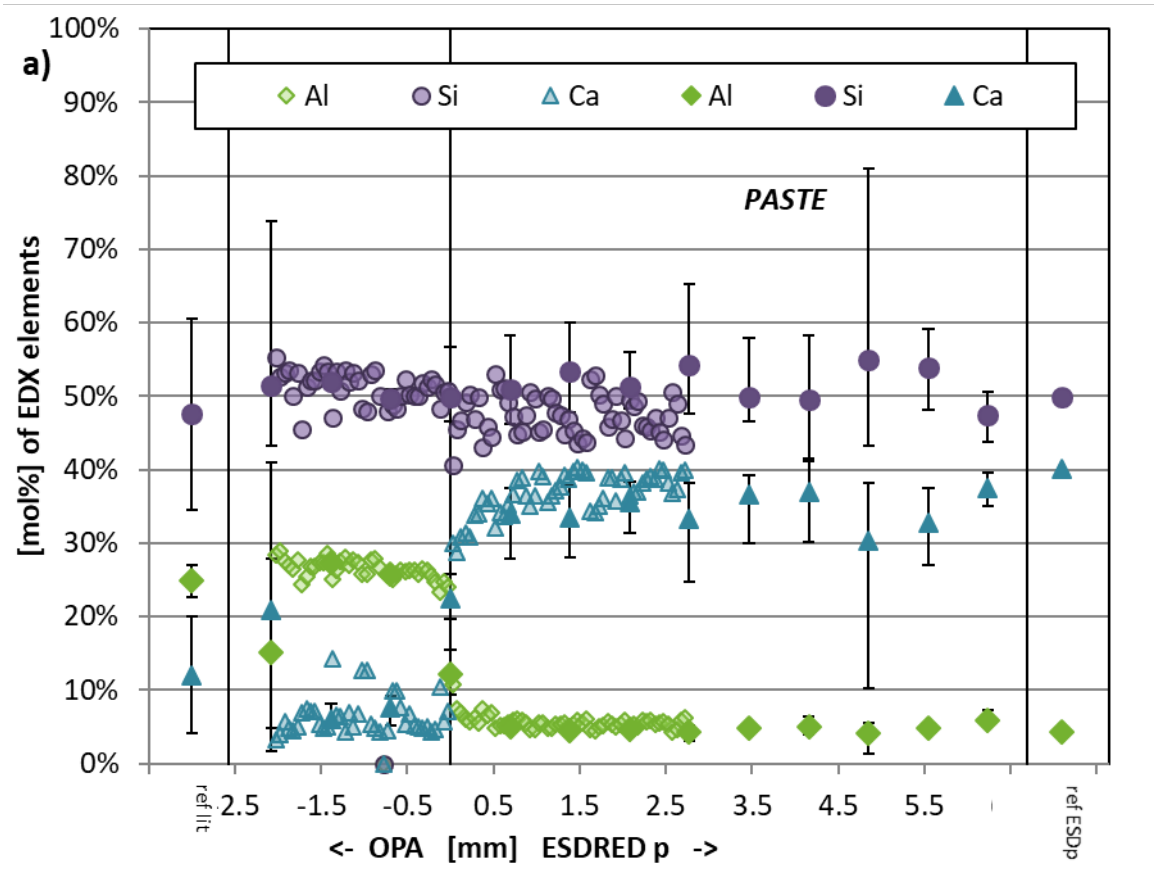

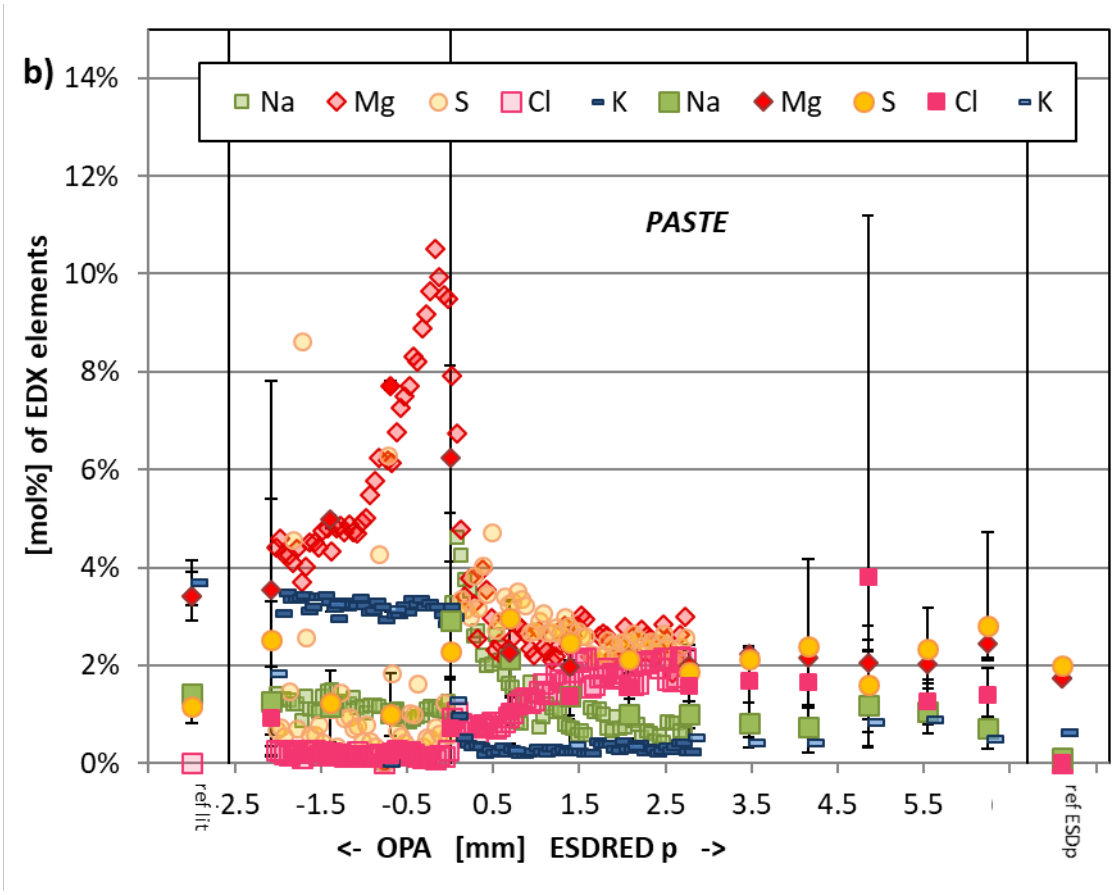
b)
Na
Mg
S
Cl
K
Na
Mg
S
Cl
K
PASTE
[mol%] of EDX elements
14%
12%
10%
8%
6%
4%
2%
0%
ref lit
-2.5
-1.5
-0.5
0.5
1.5
2.5
3.5
4.5
5.5
ref ESDp
<- OPA [mm] ESDRED p >

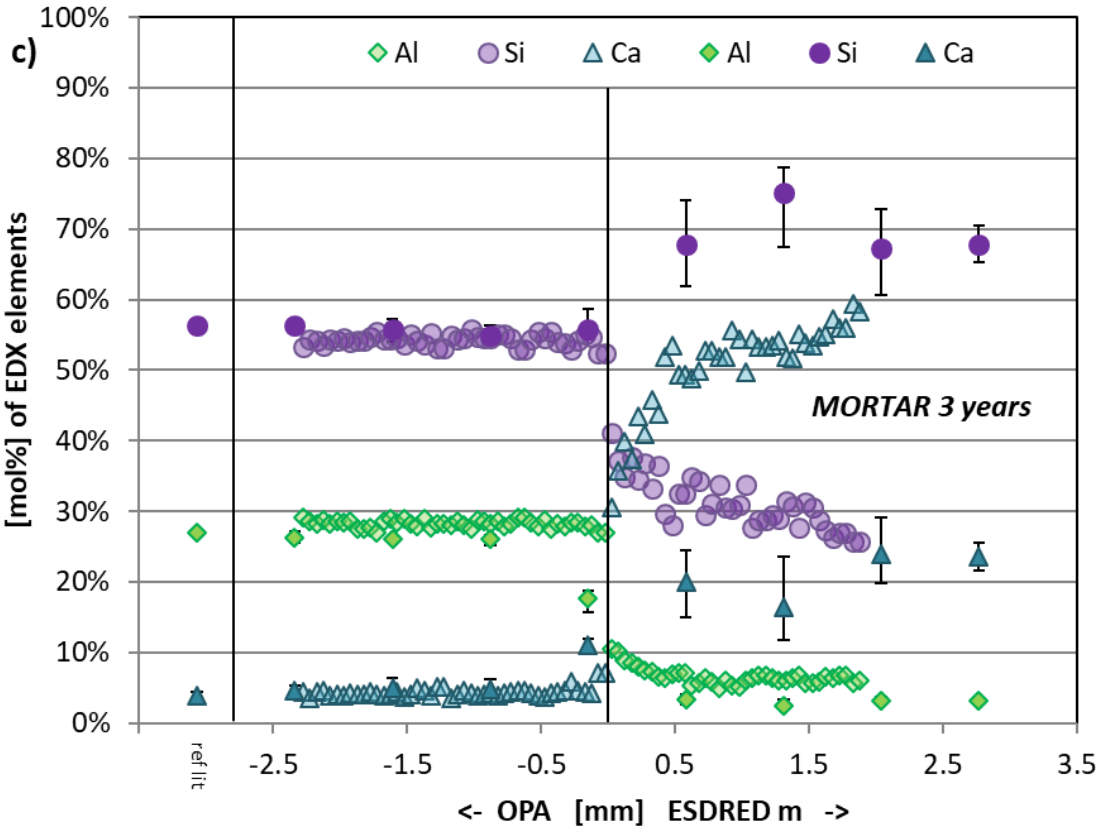
c)
Al
Si
Ca
Al
Si
Ca
100%
90%
80%
70%
60%
50%
40%
30%
20%
10%
0%
[mol%] of EDX elements
MORTAR 3 years
ref lit
-2.5
-1.5
-0.5
0.5
1.5
2.5
3.5
<- OPA [mm] ESDRED m ->
d)
Na
Mg
S
Cl
K
Na
Mg
S
Cl
K
14%
12%
10%
8%
6%
4%
2%
0%
[mol%] of EDX elements
MORTAR 3 years
ref lit
-2.5
-1.5
-0.5
0.5
1.5
2.5
3.5
<- OPA [mm] ESDRED m ->

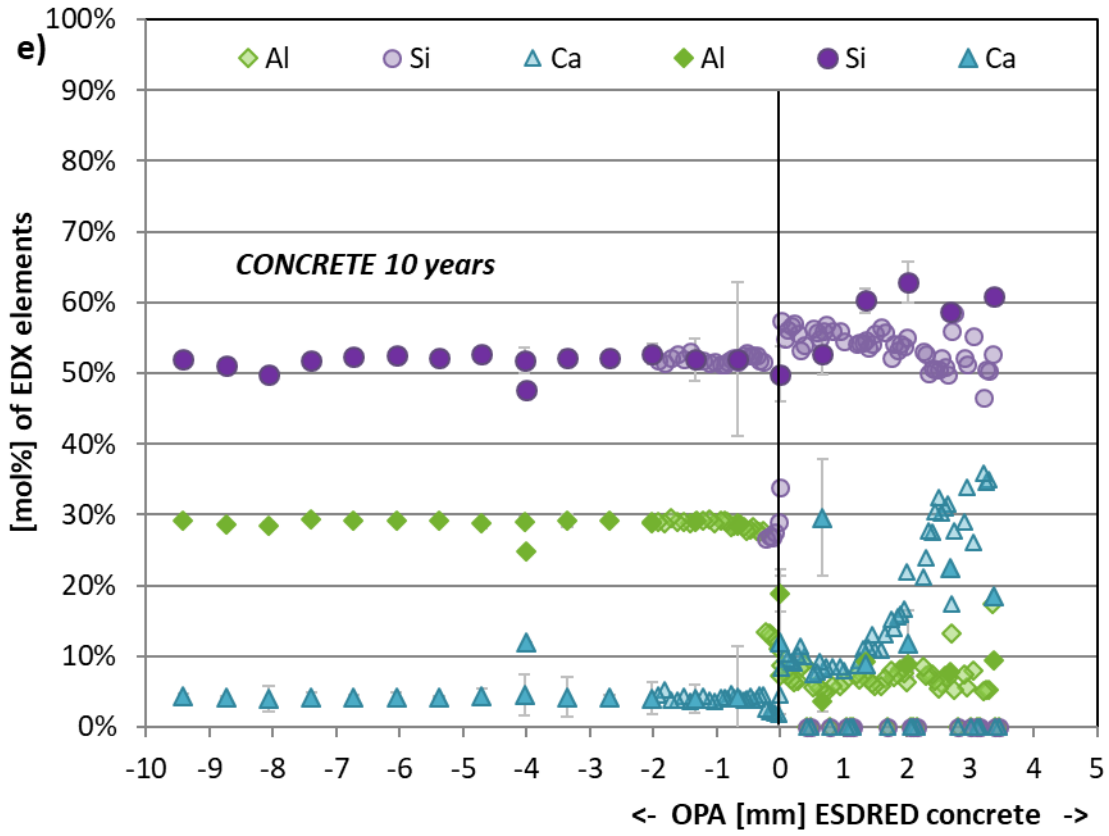
e)
Al
Si
Ca
Al
Si
Ca
CONCRETE 10 years
[mol%] of EDX elements
100%
90%
80%
70%
60%
50%
40%
30%
20%
10%
0%
-10 -9 -8 -7 -6 -5 -4 -3 -2 -1 0 1 2 3 4 5
<- OPA [mm] ESDRED concrete ->
f)
Na
Mg
S
Cl
K
Na
Mg
S
Cl
K
CONCRETE 10 years
[mol%] of EDX elements
40%
35%
30%
25%
20%
15%
10%
5%
0%
-10 -9 -8 -7 -6 -5 -4 -3 -2 -1 0 1 2 3 4 5
<- OPA [mm] ESDRED concrete ->
31

Figure 8: Profiles determined by EDS on the interface ESDRED paste (age 3.2), mortar (3.2 years) and concrete (10 years) in contact with Opalinus Clay. Dark symbols correspond to the average of one EDS map while the many light symbols correspond to the smaller step profiles of the cement pastes close to the interface, i.e. avoiding aggregates, sand, and silica fume clusters.

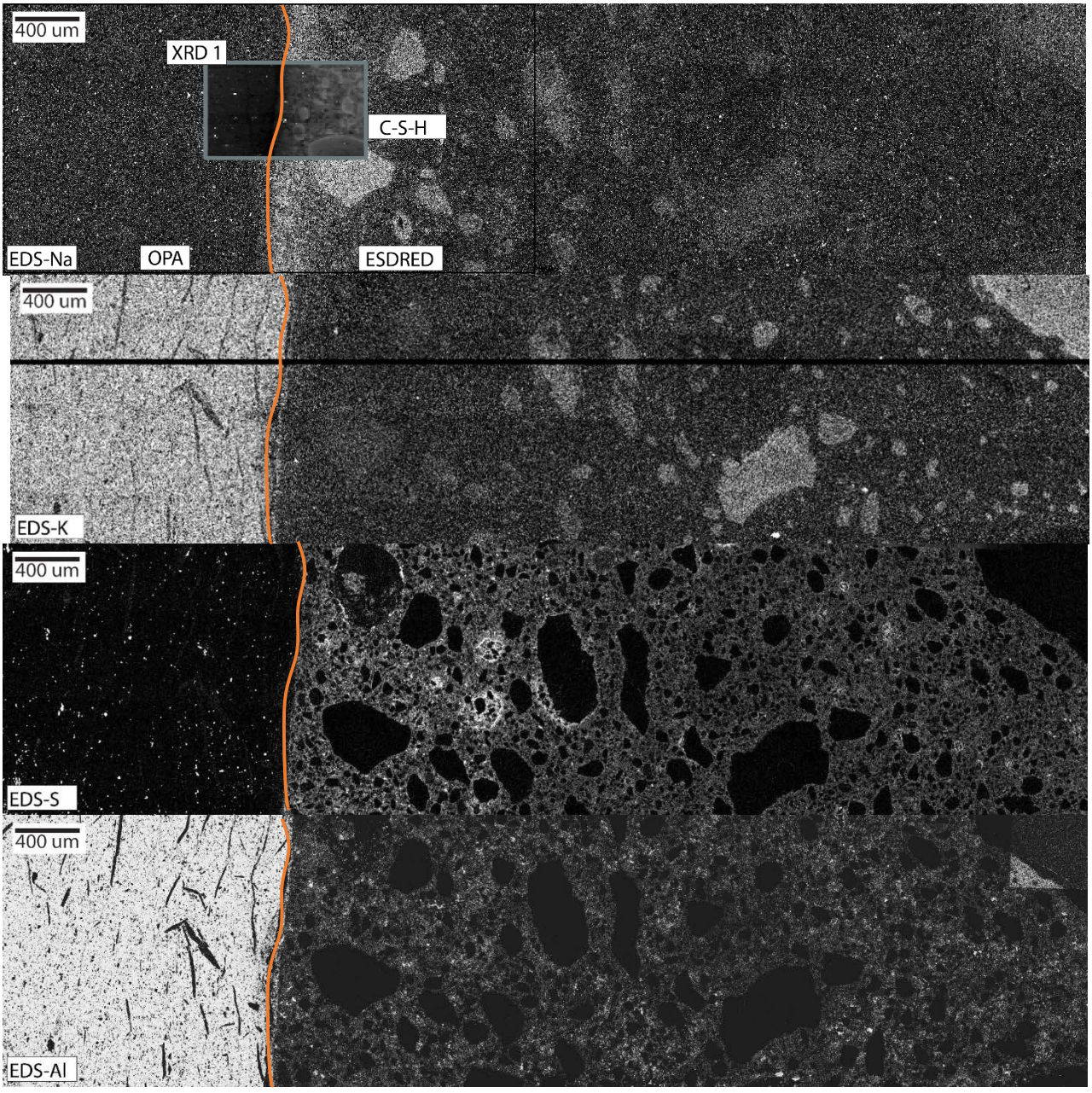

Figure 9: from top to bottom : SEM/EDS-Sodium element map and μ-XRD intensity distribution maps of C-S-H (XRD 1: small beam diameter (5 um)); SEM/EDS-Potassium element map, SEM/EDS-Sulphur element map; SEM/EDS-aluminium element map.

3.2.2. Crystallography and solid phases

The different areas analysed by µ-XRD across the interface (Figure 10a) were acquired with two different resolutions (XRD1 with 25-µm beam size, XRD2 with 5- µm). No precipitation of crystalline phases except calcite was observed near the interface and in contrast to PC paste, calcite is abundant at this interface (Figure 10a) within a thin layer of 50 µm. Up to 8 wt.% is predicted in the mortar within a 100-200 µm thick layer at the interface (supplementary material).

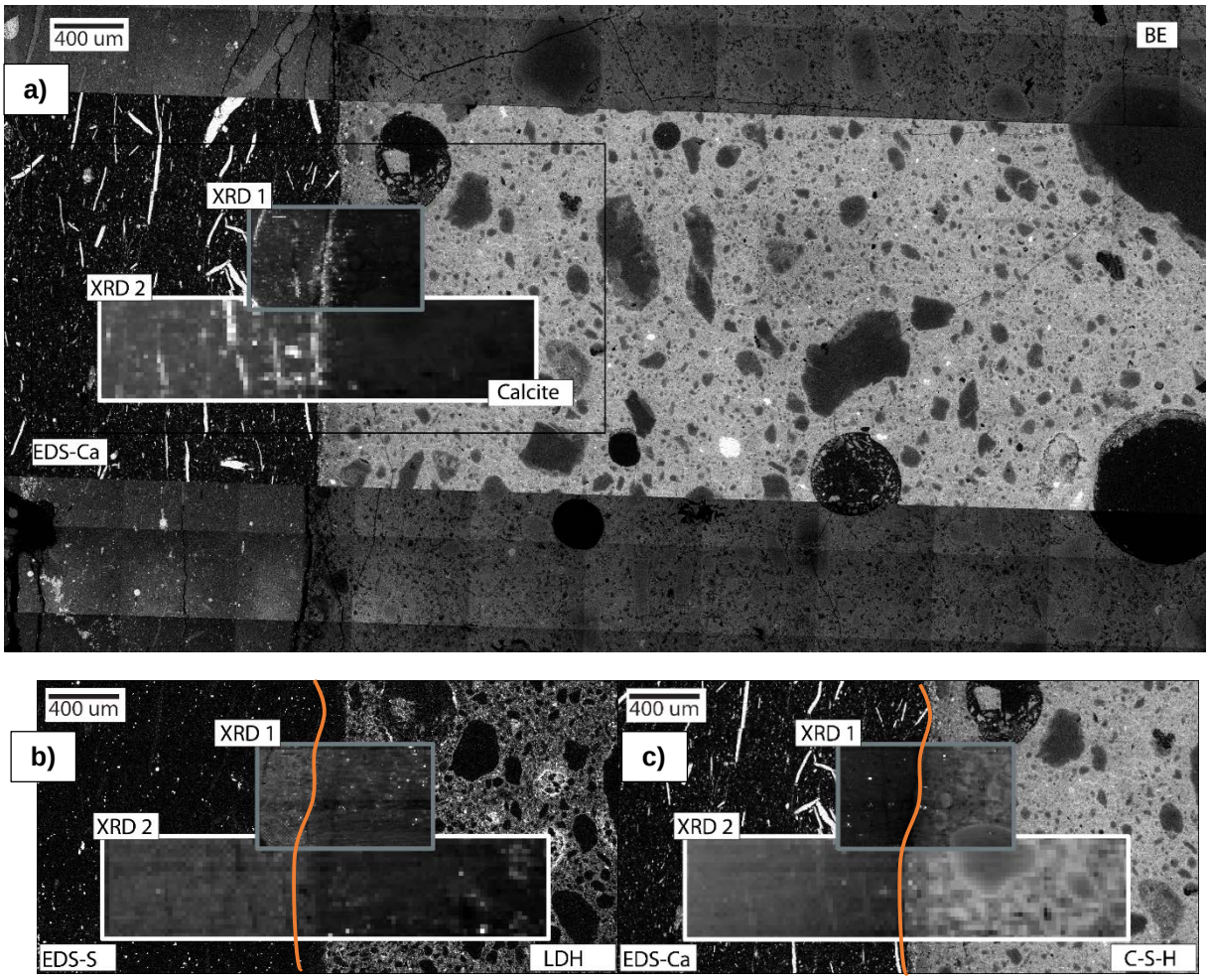

Figure 10: a) SEM/EDS-Calcium element map and calcite µ-XRD intensity distribution maps (top: 5µm-beam size bottom: 25µm-beam size); interface between Opalinus Clay (left) and ESDRED cement paste (right), aged of 3.2 years; b) SEM/EDS-Calcium element map and µ-XRD intensity distribution maps of C-S-H and c) SEM/EDS-Sulphur element map and µ-XRD intensity distribution maps of LDH (top: 5µm-beam size bottom: 25µm-beam size); the orange line indicates the interface between Opalinus Clay (left) and ESDRED cement paste (right), aged of 3.2 years.

3.2.2.1. C-S-H

ESDRED – and similar "low-pH" cements - are mainly composed of calcium silicate hydrate (C-S-H) and ettringite, in the absence of portlandite. The pH value of the pore solution is not buffered by portlandite; measured and modelled pH values are near 12 after a relatively short hydration time at closed-system conditions (Lothenbach et al., 2014). The presence of silica-rich additives promotes a lower pH and the reacted silica lowers also the Ca/Si ratio in C-S-H. In the µ-XRD intensity distribution map of C-S-H (Figure 10b), the detection of C-S-H is less clear than for well crystalline phases like clay minerals. C-S-H content in the cement matrix was quantified to be between 80 and 100 wt.% (supplementary material). It seems that the content of C-S-H is lower within 200 µm from the interface. C-S-H was also observed in the outer rim of silica fume aggregate due to a "second" or continuous hydration of the silica fume aggregate.

3.2.2.2. N-(A-)S-H and K-(A-)S-H

Interestingly, the ESDRED cement paste contains elevated sodium close to the interface while the potassium content is lower. Sodium is enriched at the very interface and within 1.5-2 mm from the interface, and potassium further away (Figure 9). The enrichment is taking place at the very interface and also in the former silica fume grains to possibly form N-(A-)S-H and K-(A-)S-H gel usually described in the alkali-silica reaction, and this may be a zeolite-precursor phase (Shi et al., 2019) and/or seems to be uptaken by the decalcified C-S-H (L'Hôpital et al., 2016).

The concentration of potassium in the ESDRED pore water is initially higher than sodium (3 times), but this is decreasing with time from 185 to 15 mmol/L after 3 years (Lothenbach et al., 2014). The free potassium ions would have reacted initially with the silica fume agglomerates and in a second stage, the sodium from the pore water in the OPA and the substantial inventory on the clay exchanger diffuse across the interface and replace the potassium in silica gels.

Small amounts of aluminium may be derived from a very minor degradation of clay or feldspar material at the interface. Zeolite-like phases have already been observed in the alkali-activation of aluminosilicates (García-Lodeiro et al., 2011; Ruiz-Santaquiteria et al., 2012) or as a degradation product during the study of aluminosilicate minerals in contact with alkaline cement pore solution (Gaucher and Blanc, 2006; Savage et al., 2007). The content of aluminium is rather low in the silica fume clusters (Figure 9), and therefore, the formation of N-S-H or K-S-H gels without aluminium as described in the alkali-silica reaction (Glasser and Kataoka, 1981) is rather occurring further away from the interface.

3.2.2.3. Sulphate phases

A sulphur enrichment of 2-2.5 mm width in the hydrated cement paste at the interface is observed by SEM/EDS (Figure 8 and Figure 10c). No µ-XRD intensity distribution maps for ettringite could be produced because the reflection peaks could not be detected in this zone. It might be that ettringite was not present at the interface in accordance with depletion of calcium (Figure 8). However, it was also difficult to observe ettringite further away from the interface. Either the lower pH of this paste might decrease the crystallinity of the ettringite, or the sample preparation might have damaged it, or only a small amount was present, or ettringite was completely destabilized at the *in situ* conditions. Preliminary results on the infiltration of artificial OPA pore water through an ESDRED mortar core sample showed that aliquots were undersaturated with respect to ettringite while oversaturated with respect to C-S-H. In the paste sample (Figure 10c) or mortar sample (supplementary material) the presence of an LDH-like phase is observed further way from the interface similar to the hydrated PC case. Gypsum, anhydrite, or basanite could not be detected.

3.2.2.4. Additional minerals in the low pH cement

The conventional XRD patterns on a successively abrased sample (Figure 11) in cement near the interface contain illite and kaolinite as contamination from OPA. Far from the interface (9 mm), C-S-H with broad reflections was observed. Ettringite and possibly monosulphate were detected in the mortar, and this confirms very low amounts in the ESDRED cement paste after 3.2 years of interaction with OPA. Only C-S-H was seen closer to the interface up to 0.15 mm. Calcite was observed at the interface and further away with the main reflections at 29.5 and 39.4 ° 2θ. Some of the calcite at the interface and at 0.15 mm is attributed to OPA, as are traces of illite and/or kaolinite. However, the depth of calcite formation in the ESDRED is larger than the perturbation of OPA, and this calcite would be formed *in situ,* from the decalcification of the C-S-H phase and the ingress of bicarbonate.

In the ESDRED cement very close to OPA, no C-S-H or cement phases were detected by conventional XRD. In this high magnesium zone (SEM/EDS), the XRD hump characteristic of the neoformation of a hydrated magnesium silicate phase was observed. Described in literature (Dauzères et al., 2016; Lerouge et al., 2017) from ESDRED concrete, a magnesium enrichment at the interface is one characteristic for low pH cementitious material in contact with OPA. This enrichment of magnesium was attributed to the precipitation of magnesium silicate hydrate. It was recently studied and has a variable Mg/Si ratio and a layered structure like a phyllosilicate. It is an extremely fine-grained or disordered talc-like or stevensite-like clay mineral, possibly mixed with minerals from a precursor of a serpentine group such as lizardite or antigorite. The characteristic pattern of this synthetic nano-crystalline neo-formed magnesium silicate hydrate has its highest reflection peak at ~19.5 ° 2θ (Cu) (Bernard et al., 2019a).

In the paste, however, the magnesium enrichment took place at the interface but more on the OPA side than the paste side (Figure 8), and this makes the observation of the

reflection at ~ 19.5 ° 2θ almost impossible with the high background of the patterns of clay phases as detailed below.

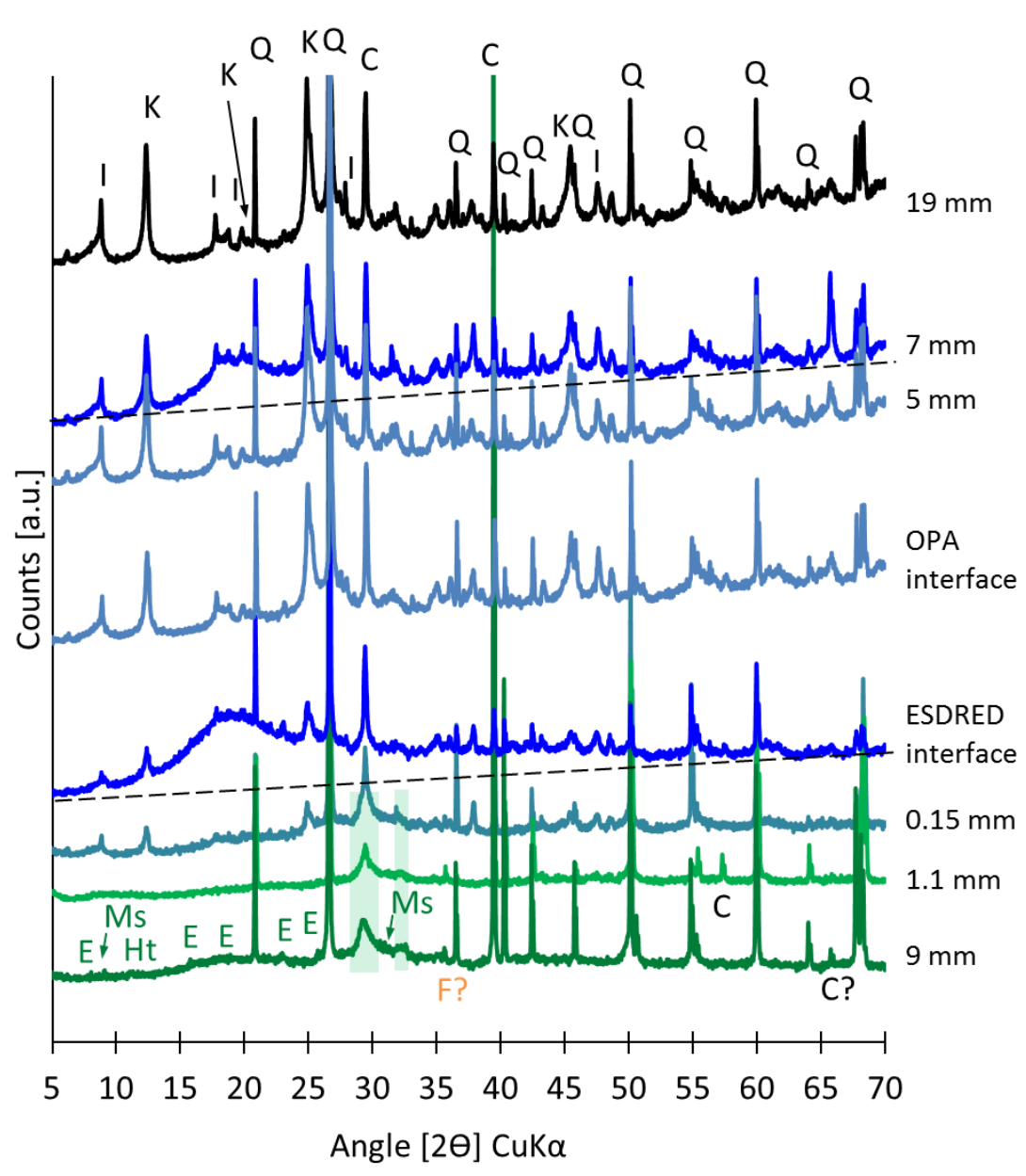

Figure 11: XRD patterns of slices in Opalinus Clay and ESDRED mortar across the interface at the different distances; green lighted area=C-S-H, C=calcite, Q=quartz, I=illite, K=kaolinite, E=ettringite, Ms=monosulfate, F=Fe_2O_3.

Generally, similar phases were observed in pastes and mortars at the interface with OPA. The presence of ettringite or monosulphate is suggested by conventional XRD compared to µ-XRD data.

3.2.2.5. Crystalline phases in Opalinus Clay and magnesium enrichment

The main crystalline minerals in OPA (chlorite, pyrite, kaolinite, illite, and quartz in Figure 12 or calcite in Figure 10a) were found by µ-XRD. Dolomite, ankerite, siderite, or illite/smectite mixed layers were difficult to observe. No clear indication for the dissolution of clay phases was observed in contact with the hydrated cement paste. The very low amount of dissolved clay expected is below the sensitivity of µ-XRD. This was confirmed by conventional XRD of the mortar on slices far from the interface (19 mm) in Figure 11, where the OPA pattern exhibits a characteristic reflection of the major minerals as illite (and illite/smectite), kaolinite, calcite, and quartz. The detection of the other minor minerals was difficult.

The patterns recorded at 5 and 7 mm from the interface and directly adjacent to the interface were very comparable to the undisturbed OPA observed at 19 mm distance, except for the pattern at 7 mm which showed an asymmetric broad hump located at ~ 19° 2θ. This signal could be related to the formation of Mg-Si hydrates in the OPA. However, in all ESDRED-OPA interfaces studied so far, magnesium in OPA was enriched right at the interface, and never distant from the interface (Dauzères et al., 2016; Jenni et al., 2014; Mäder et al., 2017).

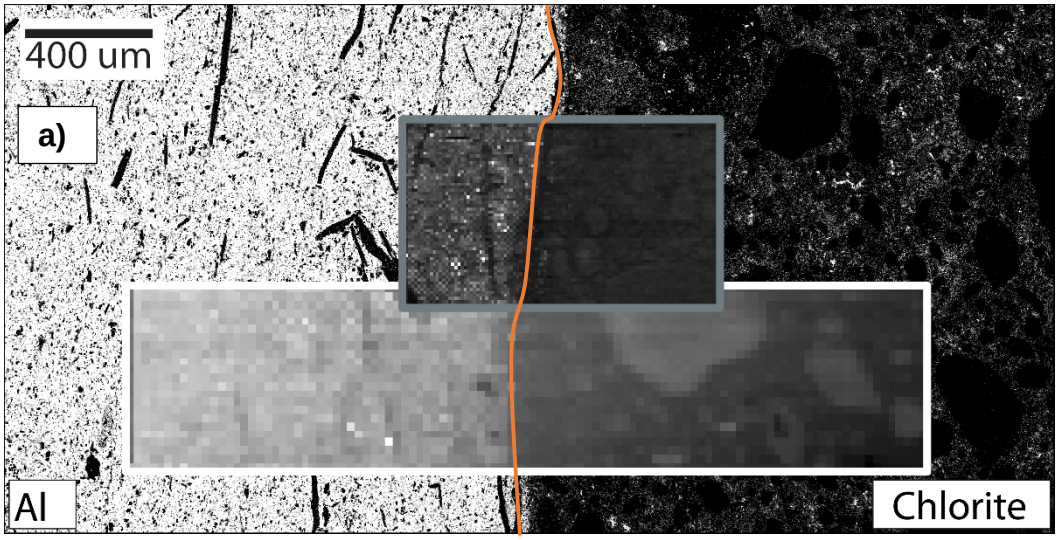
400 um
a)
Al
Chlorite

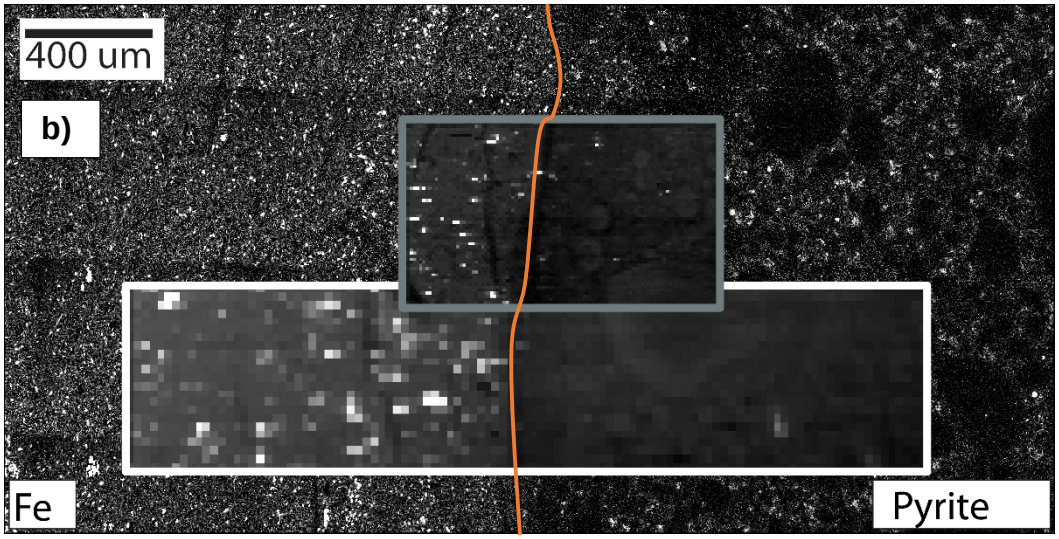
400 um
b)
Fe
Pyrite

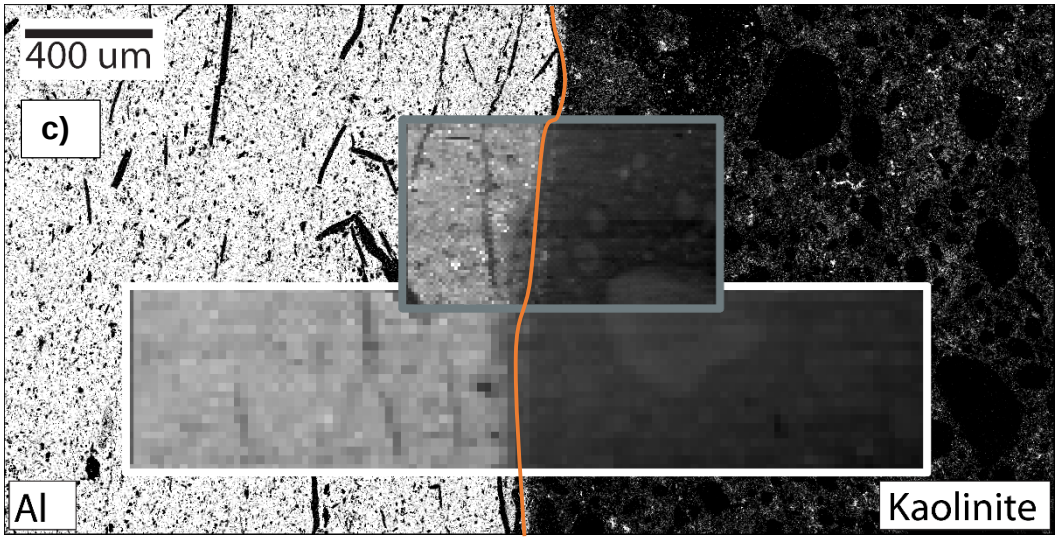
400 um
c)
Al
Kaolinite

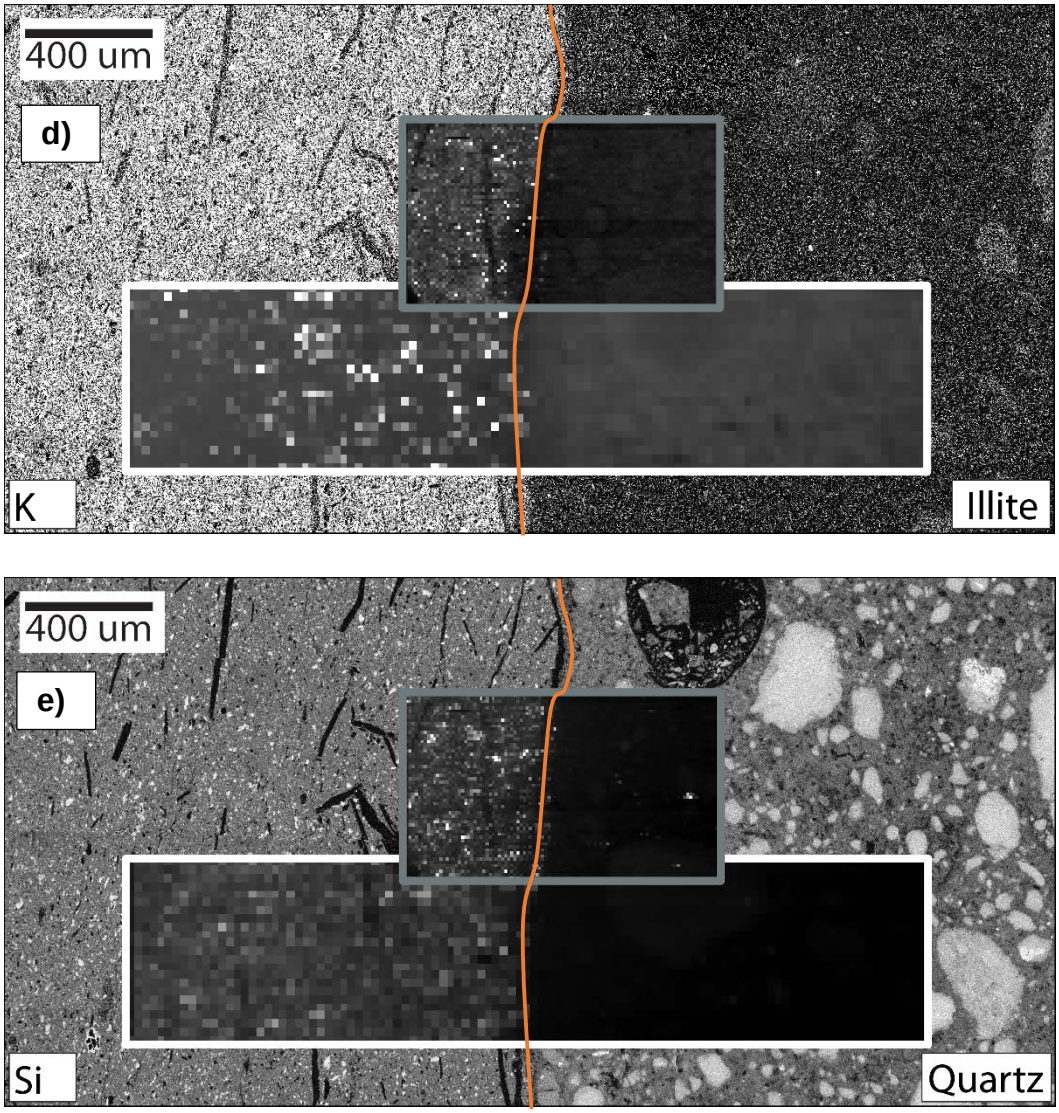

Figure 12: SEM/EDS maps (Al, Fe, K, Si) and µ-XRD intensity distribution maps of a) chlorite, b) pyrite, c) kaolinite, d) illite, and e) quartz (top: 5µm-beam size bottom: 25µm-beam size); the orange line indicates the interface between Opalinus Clay (left) and ESDRED cement paste (right), aged of 3.2 years.

4. Conclusions

4.1. Methodology and mineral distributions

This µ-XRD campaign resulted in conclusive and spatially resolved µ-XRD measurements. Special attention was paid to the distribution of crystalline phases in order to assess open questions with regard to variations in elemental concentrations near the interface obtained in the past studies by SEM/EDS (Dauzères et al., 2014; Jenni et al., 2017; Jenni et al., 2014; Lerouge et al., 2017; Mäder et al., 2017). The

main characteristic cement hydrates C-S-H, portlandite or ettringite could be found in the samples, and mechanisms of their partial or total dissolution in contact with the OPA was confirmed. This study profited from a drastically improved sample preparation that resulted in better diffraction data with respect to the previous investigations, but also from in-depth crystallographic data treatment approaches.

Portlandite, ettringite and C-S-H contained in the PC paste were partially or completely absent in contact with the OPA. C-S-H and ettringite were present in the undisturbed ESDRED and similarly to PC paste, they were destabilized at the interface. Interestingly, neither ettringite nor other sulphur-bearing crystalline phases could be found in the ESDRED. Contrary to the former studies with concretes or mortars, calcite was not observed at the interface PC paste - OPA while well observed at the interface ESDRED/low-pH cement paste – OPA and calcite was observed in the PC and low-pH cement mortars.

No crystalline phase could be detected at the location of the magnesium enrichment, because the possible nano-crystalline magnesium silicate hydrate precipitation is not present in sufficient quantities to be detected. Despite the fact that the mineral composition of the zones with increased sulphur and magnesium could not be unambiguously clarified, µ-XRD has proven a powerful tool for in-depth analysis of cementitious material - OPA interfaces. It provides information that cannot be derived from chemical analyses and allows for a sound interpretation of interaction mechanisms.

4.2. Interpretation of mechanisms

The findings of this µ-XRD campaign combined with the data from the former campaigns (Dauzères et al., 2014; Jenni et al., 2017; Jenni et al., 2014; Mäder et al., 2017) are schematically summarized in Figure 13a for the PC paste - OPA interface and in Figure 13b for the ESDRED paste - OPA interface.

The chemical and mineralogical inhomogeneities around the interfaces allow for the interpretation of processes going on during the interaction of cement and clay. Several interacting processes occur for different periods during the sample evolution. The measurements shown represent the superposition of the effects of the processes, which complicates their interpretation. The faith of *calcium* at the interface has been derived as follows:

Portland cement paste – Opalinus Clay interface:

i) continuous hydration of clinker phases at the interface due to the OPA water reservoir which increases the calcium concentration in the porewater

ii) migration of the calcium from the cement across the interface to the exchangeable clay sites of the OPA, releasing sodium to the OPA pore water, which diffuses into the cement

iii) hindered formation or complete dissolution of Portlandite up to ~0.2 mm, dissolution of ettringite up to ~1 mm and complete depletion of C-S-H up to 0.1 mm, while C-S-H content was strongly reduced to a 1 mm-depth. Low calcium activity and low pH at the interface (calcium ions and hydroxyl migrate into the OPA) cause the instability of these cement hydrates

iv) it is expected that carbon species migrate from OPA deep into the cement paste, react with calcium released from the destabilisation of the hydrates, and calcite precipitate at the interface or distributed over a wide range of distances from the interface.

ESDRED cement paste – Opalinus Clay interface:

i) continuous hydration of clinker phases, particularly of the silica fume cluster, close to the interface. The presence of silica fume buffers the silicon concentration to its solubility

ii) migration of the calcium to the exchangeable sites of the OPA, releasing sodium, which diffuses back into the cement (comparable to PC but probably slower)

iii) dissolution of C-S-H at the interface with a general decrease toward the interface and total dissolution of ettringite over a depth $\gtrsim$3 mm

iv) calcite precipitates at the very interface due to the migration of the carbon species from OPA into the cement paste, and reacts with calcium in the porewater released from the destabilisation of the cement hydrates.

The nature of the *magnesium* precipitations could not be elucidated by µ-XRD, mainly due to a low content and nano-crystalline character of the Mg-phases. The possible LDH precipitation at the interface OPA – PC paste likely contains magnesium as the LDH containing calcium are not stable at low pH values. The distance of magnesium precipitation in the OPA is mainly depending on the local pH and migration of the hydroxide ions, in turn controlled by kinetic clay dissolution.

Portland cement paste – Opalinus Clay interface:

i) Release of magnesium from the exchangeable clay sites by replacement with mostly calcium. (Fernandez et al., 2009) demonstrated the magnesium removal from the exchanger of a 2 cm clay column, and precipitation of magnesium hydrates at the end of the column in contact with high pH cement water. Minor dissolution of OPA minerals within the high pH zone close to the interface, particularly dolomite (expected from modelling (Jenni et al., 2017)), releases additional magnesium

ii) precipitation of nanocrystalline M-S-H and/or semi-amorphous Mg-LDH in the OPA away from the interface due to favorable activity of silicon, magnesium and appropriate pH (~9-11).

ESDRED cement paste – Opalinus Clay interface:

i) Release of magnesium from the exchangeable clay sites and from minimal dissolution of OPA minerals as described for the PC-OPA interface

ii) precipitation of nanocrystalline M-S-H in the cement at the interface and/or

iii) precipitation of nanocrystalline M-S-H in the magnesium-enriched OPA right at the interface.

Sodium and *aluminium* enrichments in the cement paste at the interface could not be associated to crystalline phases. They are likely due to influx from the OPA side and, at the appropriate pH, could be associated to amorphous gels, or to uptake by C-S-H observed at lower pH. The regions with increased *sulphur* are explained by the migration of the OPA pore water into the cement paste but associated minerals could not be determined by µ-XRD. It can be speculated that sulphate adsorbed on C-(N-A-)S-H or precipitated in low crystalline S-bearing LDH phase (although the S-enriched zone does not correspond to the LDH precipitation in some cases), or in gypsum or monosulphate undetectable by µ-XRD but observed in other concretes in contact with clayey materials (Tinseau et al., 2006). Further away from the interface, the higher pH allows for precipitation of S-bearing cement hydrates. At concrete-OPA interfaces, S is generally depleted in the cement close to the interface, but enriched further away (e.g., Figure 8f, 10 y of interaction), in line with the interpretation above. The S pattern might not only depend on the binder type, but also on interaction time and porosity (concrete porosity at equal w/b is smaller than in mortar).

Comparing the two different binders and their interaction with OPA in a repository context, the following differences stand out: the high pH plume generated from the PC enters further into the OPA than in case of the ESDRED-OPA interaction after 3.2 years (PC: 2-8 mm, ESDRED: 0.2-0.5 mm, both distances depending on type and age). First of all, lower pH in the ESDRED leads to a lower hydroxide ions flux into OPA. In addition, the porosity and therefore transport, possibly decreases around the ESDRED interface during the interaction: calcite and M-S-H precipitate in the interface region, and C-S-H (main cement phase in ESDRED) resists lower pH values than portlandite in PC.

Another key question in the repository performance concerns the long-term evolution of the interaction processes. The dissolution of OPA minerals at high pH, especially of the clays, is expected to occur too slow to be detected within tens of years in such complex systems. Even minimal dissolution can buffer high pH, but is kinetically controlled to slow rates. It must be expected that OPA phases will dissolve as long as cementitious material is present and controls high pH, unless porosity clogging slows down transport across the interface. This study indicates minor dissolution and precipitation and potentially clogging at the ESDRED-OPA interface, but only dissolution in case of the PC-OPA interface. However, concerning the ESDRED, the first results from time-series of interface samples up to 10 years indicate an ongoing penetration of the magnesium enrichment with the same rate between 5 and 10 years, and therefore of the pH front, into OPA.

It has been difficult so far to evaluate the porosity in *in-situ* sampled interfaces, containing both cementitious and clayey materials mainly which are strongly impeded by artefacts from sampling and drilling (Mäder et al., 2017).

The extents of reaction are different between the two cement types but are small at an absolute scale of material thicknesses, and clay dissolution could not be directly detected with mineralogical methods. Given the intrinsic tendencies towards pore space reduction, reaction progress is expected to slow down and render the compartments more and more chemically isolated. Efforts should, therefore, focus on directly constraining transport and on implementing mechanisms and coupling terms into reactive transport models correctly. While the overall effects may be small in terms of mass transfers, the local changes to the pore network may affect gas transport, for example, that in turn may be an issue for certain repository designs and waste forms.

An alternative approach is to directly examine the transport effects of such interfaces at the field scale by a diffusion experiment with appropriate tracers (^{3}H, ^{36}Cl, for example), and examine subsequently tracer profiles across the interface. Such an experiment was started at Mont Terri recently (named CI-D), taking advantage of the existing aged cementitious materials described in this study.

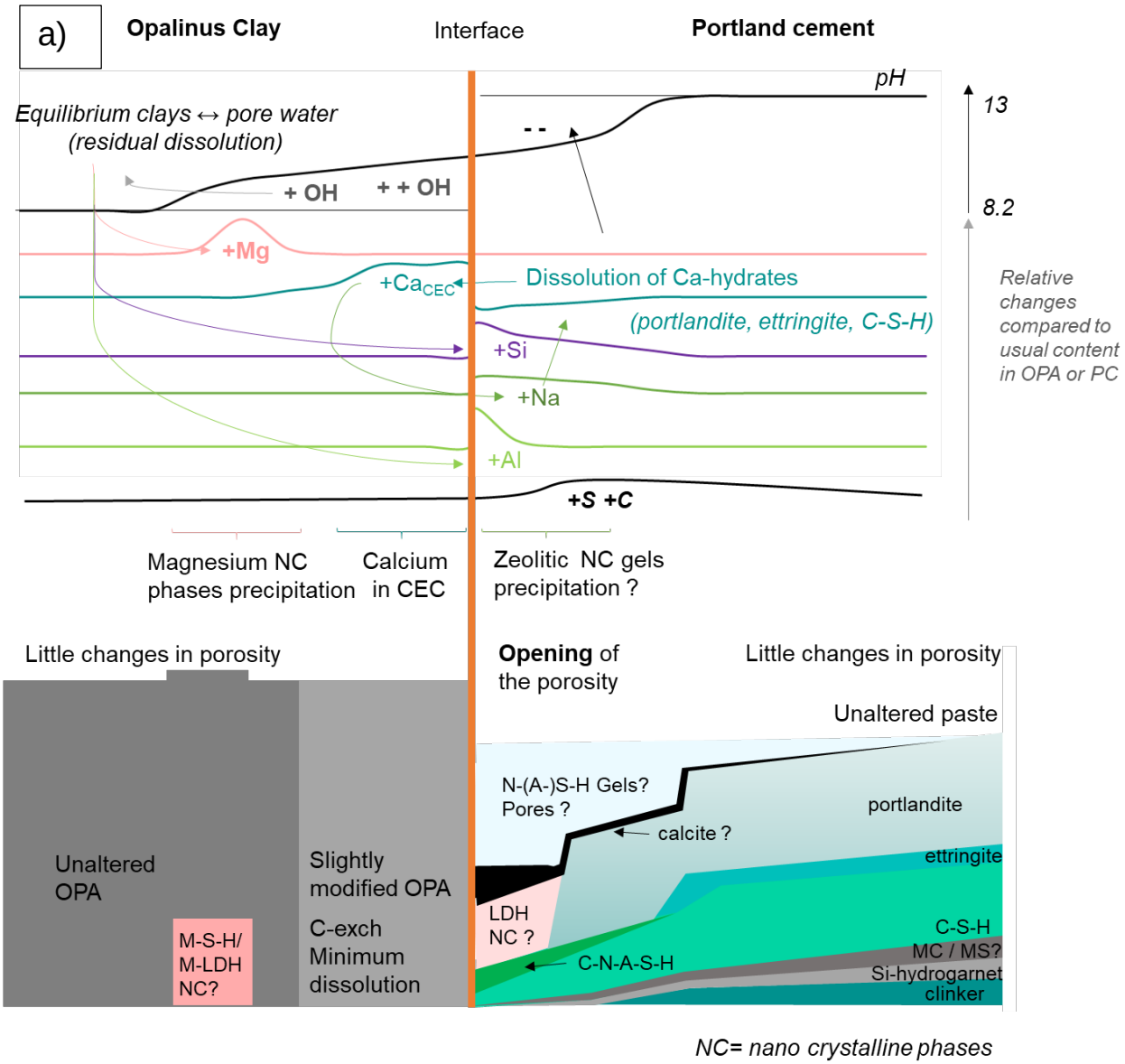

NC= nano crystalline phases

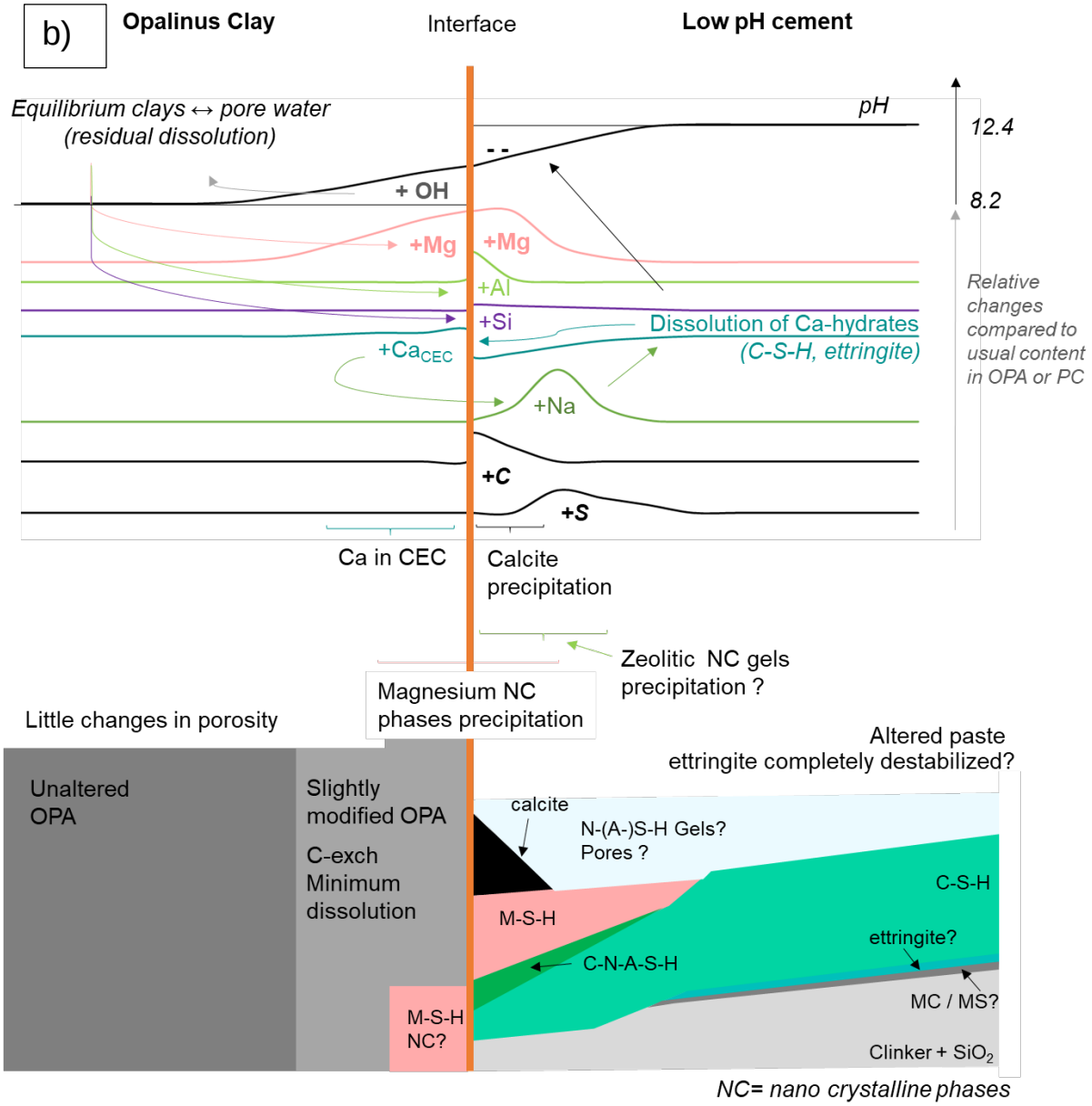

Figure 13: Schematic overviews of the phases observed by μ-XRD together with the SEM/EDS data from the former campaigns ("?" correspond to the possible explanation of the SEM/EDS data, but not confirmed by μ-XRD) ; sulphur faith has been excluded MC/MS= mono/hemi-carbonate, mono/hemi-sulphate, a) Opalinus Clay – Portland cement paste interface, b) Opalinus Clay – ESDRED paste interface.

Acknowledgements

Most of the analytical results presented here rely on samples carefully crafted by the rock preparation team of the Institute of Geological Sciences, University of Bern. The CI Project is funded by ANDRA, CRIEPI, IRSN, FANC, Nagra, Obayashi, and SCK-CEN. It financed all drilling campaigns, part of sample preparation, and earlier analytical costs. The scientific and technical team operating the Mont Terri facility (Swisstopo) is acknowledged for field support. The teams of the SLS X05LA microXAS beamline and of the ESRF SNBL BM01 beamline are both acknowledged for their great 24 h support during the measurement campaigns.

5. References

Adler, M., Mäder, U., Waber, H.N., 1999. High-pH alteration of argillaceous rocks: an experimental study. Schweiz. Mineral. Petrogr. Mitt 79, 445-454.

Allen, A.J., Thomas, J.J., Jennings, H.M., 2007. Composition and density of nanoscale calcium–silicate–hydrate in cement. Nature materials 6, 311-316.

ANDRA, 2005. Evaluation of the feasibility of a geological repository in an argillaceous formation. Collection Les rapports 2005.

Bach, T., Chabas, E., Pochard, I., Cau Dit Coumes, C., Haas, J., Frizon, F., Nonat, A., 2013. Retention of alkali ions by hydrated low-pH cements: Mechanism and Na^+/K^+ selectivity. Cement and Concrete Research 51, 14-21.

Barbarulo, R., 2002. Comportement des matériaux cimentaires: actions des sulfates et de la température, Université Laval Québec.

Bartier, D., Techer, I., Dauzères, A., Boulvais, P., Blanc-Valleron, M.-M., Cabrera, J., 2013. In situ investigations and reactive transport modelling of cement paste/argillite interactions in a saturated context and outside an excavated disturbed zone. Applied Geochemistry 31, 94-108.

Bauer, A., Berger, G., 1998. Kaolinite and smectite dissolution rate in high molar KOH solutions at 35 and 80 C. Applied Geochemistry 13, 905-916.

Bernard, E., Lothenbach, B., Cau-Dit-Coumes, C., Chlique, C., Dauzères, A., Pochard, I., 2018. Magnesium and calcium silicate hydrates, Part I: Investigation of the possible magnesium incorporation in calcium silicate hydrate (C-S-H) and of the calcium in magnesium silicate hydrate (M-S-H). Applied Geochemistry 89, 229-242.

Bernard, E., Lothenbach, B., Chlique, C., Wyrzykowski, M., Dauzères, A., Pochard, I., Cau-Dit-Coumes, C., 2019a. Characterization of magnesium silicate hydrate (M-S-H). Cement and Concrete Research 116, 309-330.

Bernard, E., Lothenbach, B., Le Goff, F., Pochard, I., Dauzères, A., 2017. Effect of magnesium on calcium silicate hydrate (C-S-H). Cement and Concrete Research 97, 61-72.
Bernard, E., Lothenbach, B., Pochard, I., Cau-dit-Coumes, C., 2019b. Alkali binding by magnesium silicate hydrates. Journal of the American Ceramic Society 00, 1–15.
Berner, U., 1992. Evolution of pore water chemistry during degradation of cement in a radioactive waste repository environment. Waste Management 12, 201-219.
Cau Dit Coumes, C., Courtois, S., Nectoux, D., Leclercq, S., Bourbon, X., 2006. Formulating a low-alkalinity, high-resistance and low-heat concrete for radioactive waste repositories. Cement and Concrete Research 36, 2152-2163.
Cavani, F., Trifiro, F., Vaccari, A., 1991. Hydrotalcite-type anionic clays: Preparation, properties and applications. Catalysis today 11, 173-301.
Claret, F., Bauer, A., Schäfer, T., Griffault, L., Lanson, B., 2002. Experimental investigation of the interaction of clays with high-pH solutions: A case study from the Callovo-Oxfordian formation, Meuse-Haute Marne underground laboratory (France). Clays and Clay Minerals 50, 633-646.
Codina, M., Cau-dit-Coumes, C., Le Bescop, P., Verdier, J., Ollivier, J., 2008. Design and characterization of low-heat and low-alkalinity cements. Cement and Concrete Research 38, 437-448.
Dauzères, A., Achiedo, G., Nied, D., Bernard, E., Alahrache, S., Lothenbach, B., 2016. Magnesium perturbation in low-pH concretes placed in clayey environment - solid characterizations and modeling. Cement and Concrete Research 79, 137-150.
Dauzères, A., Achiedo, G., Nied, D., L'Hopital, E., Alahrache, S., Lothenbach, B., 2014. M-S-H precipitation in low-pH concrete in clayey environment. Nuwcem 2014, Avignon.
De Nolf, W., Vanmeert, F., Janssens, K., 2014. XRDUA: crystalline phase distribution maps by two-dimensional scanning and tomographic (micro) X-ray powder diffraction. Journal of applied crystallography 47, 1107-1117.
De Weerdt, K., Justnes, H., 2015. The effect of sea water on the phase assemblage of hydrated cement paste. Cement and Concrete Composites 55, 215-222.
Fernandez, R., Maeder, U.K., Rodriguez, M., Vigil de la Villa, R., Cuevas, J., 2009. Alteration of compacted bentonite by diffusion of highly alkaline solutions. Eur J Mineral 21, 725-735.
Fernández, R., Rodríguez, M., de la Villa, R.V., Cuevas, J., 2010. Geochemical constraints on the stability of zeolites and C–S–H in the high pH reaction of bentonite. Geochimica et Cosmochimica Acta 74, 890-906.
García-Lodeiro, I., Palomo, A., Fernández-Jiménez, A., Macphee, D., 2011. Compatibility studies between NASH and CASH gels. Study in the ternary diagram Na_2O–CaO–Al_2O_3–SiO_2–H_2O. Cement and Concrete Research 41, 923-931.
Gaucher, E.C., Blanc, P., 2006. Cement/clay interactions–a review: experiments, natural analogues, and modeling. Waste Management 26, 776-788.

Glasser, L.D., Kataoka, N., 1981. The chemistry of 'alkali-aggregate'reaction. Cement and concrete research 11, 1-9.
Haas, J., 2012. Etude expérimentale et modélisation thermodynamique du système $CaO\text{-}SiO_2\text{-}(Al_2O_3)\text{-}H_2O$. Université de Bourgogne.
Halamickova, P., Detwiler, R.J., Bentz, D.P., Garboczi, E.J., 1995. Water permeability and chloride ion diffusion in Portland cement mortars: relationship to sand content and critical pore diameter. Cement and concrete research 25, 790-802.
Jacques, D., Wang, L., Martens, E., Mallants, D., 2010. Modelling chemical degradation of concrete during leaching with rain and soil water types. Cement and Concrete Research 40, 1306-1313.
Jenni, A., Gimmi, T., Alt-Epping, P., Mäder, U., Cloet, V., 2017. Interaction of ordinary Portland cement and Opalinus Clay: Dual porosity modelling compared to experimental data. Physics and Chemistry of the Earth, Parts A/B/C.
Jenni, A., Mäder, U., Lerouge, C., Gaboreau, S., Schwyn, B., 2014. In situ interaction between different concretes and Opalinus clay. Physics and Chemistry of the Earth, Parts A/B/C 70, 71-83.
L'Hôpital, E., Lothenbach, B., Scrivener, K., Kulik, D., 2016. Alkali uptake in calcium alumina silicate hydrate (CASH). Cement and Concrete Research 85, 122-136.
Lalan, P., Dauzères, A., De Windt, L., Bartier, D., Sammaljärvi, J., Barnichon, J.-D., Techer, I., Detilleux, V., 2016. Impact of a 70° C temperature on an ordinary Portland cement paste/claystone interface: An in situ experiment. Cement and Concrete Research 83, 164-178.
Leisinger, S.M., Bhatnagar, A., Lothenbach, B., Johnson, C.A., 2014. Solubility of chromate in a hydrated OPC. Applied Geochemistry 48, 132-140.
Lerouge, C., Gaboreau, S., Grangeon, S., Claret, F., Warmont, F., Jenni, A., Cloet, V., Mäder, U., 2017. In situ interactions between Opalinus Clay and Low Alkali Concrete. Physics and Chemistry of the Earth, Parts A/B/C 99, 3-21.
Lothenbach, B., Bary, B., Le Bescop, P., Schmidt, T., Leterrier, N., 2010. Sulfate ingress in Portland cement. Cement and Concrete Research 40, 1211-1225.
Lothenbach, B., Bernard, E., Mäder, U., 2017. Zeolite formation in the presence of cement hydrates and albite. Physics and Chemistry of the Earth, Parts A/B/C 99, 77-94.
Lothenbach, B., Kulik, D.A., Matschei, T., Balonis, M., Baquerizo, L., Dilnesa, B., Miron, G.D., Myers, R.J., 2018. Cemdata18: A chemical thermodynamic database for hydrated Portland cements and alkali-activated materials. Cement and Concrete Research.
Lothenbach, B., Le Saout, G., Ben Haha, M., Figi, R., Wieland, E., 2012. Hydration of a low-alkali CEM III/B–SiO2 cement (LAC). Cement and Concrete Research 42, 410-423.

Lothenbach, B., Rentsch, D., Wieland, E., 2014. Hydration of a silica fume blended low-alkali shotcrete cement. Physics and Chemistry of the Earth, Parts A/B/C 70, 3-16.
Lothenbach, B., Winnefeld, F., 2006. Thermodynamic modelling of the hydration of Portland cement. Cem Concr Res 36, 209-226.
Mäder, U., Jenni, A., Lerouge, C., Gaboreau, S., Miyoshi, S., Kimura, Y., Cloet, V., Fukaya, M., Claret, F., Otake, T., Shibata, M., Lothenbach, B., 2017. 5-year chemico-physical evolution of concrete-claystone interfaces. Swiss Journal of Geosciences 110, 307-327.
Matschei, T., Lothenbach, B., Glasser, F., 2007. The AFm phase in Portland cement. Cement and Concrete Research 37, 118-130.
Miyata, S., 1983. Anion-exchange properties of hydrotalcite-like compounds. Clays and Clay Minerals 31, 305-311.
Myers, R.J., Lothenbach, B., Bernal, S.A., Provis, J.L., 2015. Thermodynamic modelling of alkali-activated slag cements. Applied Geochemistry 61, 233-247.
NAGRA, 2002. Demonstration of feasibility of disposal ("Entsorgungsnachweis") for spent fuel, vitrified high-level waste and long-lived intermediate-level waste. Opalinus Clay Project.
Nied, D., Enemark-Rasmussen, K., L'Hopital, E., Skibsted, J., Lothenbach, B., 2016. Properties of magnesium silicate hydrates (MSH). Cement and Concrete Research 79, 323-332.
Nishikawa, T., Suzuki, K., Ito, S., Sato, K., Takebe, T., 1992. Decomposition of synthesized ettringite by carbonation. Cement and Concrete Research 22, 6-14.
Ramírez, S., Cuevas, J., Vigil, R., Leguey, S., 2002. Hydrothermal alteration of "La Serrata" bentonite (Almeria, Spain) by alkaline solutions. Applied Clay Science 21, 257-269.
Ruiz-Santaquiteria, C., Skibsted, J., Fernández-Jiménez, A., Palomo, A., 2012. Alkaline solution/binder ratio as a determining factor in the alkaline activation of aluminosilicates. Cement and Concrete Research 42, 1242-1251.
Savage, D., Walker, C., Arthur, R., Rochelle, C., Oda, C., Takase, H., 2007. Alteration of bentonite by hyperalkaline fluids: A review of the role of secondary minerals. Physics and Chemistry of the Earth, Parts A/B/C 32, 287-297.
SCK • CEN, 2012. Preparatory safety assessment. Conceptual model description of the reference case. ER-215, CCHO - 2009-00940000, SCK • CEN, Mol, Belgium.
Shi, Z., Geng, G., Leemann, A., Lothenbach, B., 2019. Synthesis, characterization, and water uptake property of alkali-silica reaction products. Cement and Concrete Research 121, 58-71.
Skinner, L., Chae, S., Benmore, C., Wenk, H., Monteiro, P., 2010. Nanostructure of calcium silicate hydrates in cements. Physical review letters 104, 195502.
Swanton, S., Heath, T., Clacher, A., 2016. Leaching behaviour of low Ca: Si ratio $CaO–SiO_2–H_2O$ systems. Cement and Concrete Research 88, 82-95.

Techer, I., Bartier, D., Boulvais, P., Tinseau, E., Suchorski, K., Cabrera, J., Dauzères, A., 2012. Tracing interactions between natural argillites and hyper-alkaline fluids from engineered cement paste and concrete: Chemical and isotopic monitoring of a 15-years old deep-disposal analogue. Applied Geochemistry 27, 1384-1402.
Tinseau, E., Bartier, D., Hassouta, L., Devol-Brown, I., Stammose, D., 2006. Mineralogical characterization of the Tournemire argillite after in situ interaction with concretes. Waste Management 26, 789-800.
Vollpracht, A., Lothenbach, B., Snellings, R., Haufe, J., 2015. The pore solution of blended cements: a review. Materials and Structures, 1-27.